

AD-A179 736

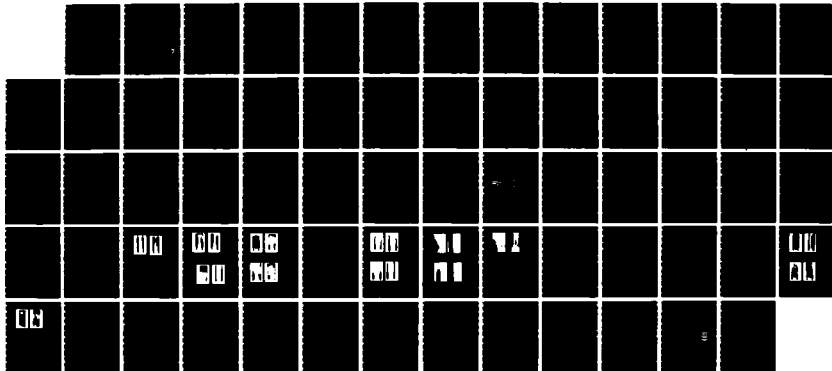
ANNULAR LIQUID PROPELLANT JETS - INJECTION ATOMIZATION
AND IGNITION(U) ARMY BALLISTIC RESEARCH LAB ABERDEEN
PROVING GROUND MD A BIRK ET AL MAR 87 BRL-TR-2788

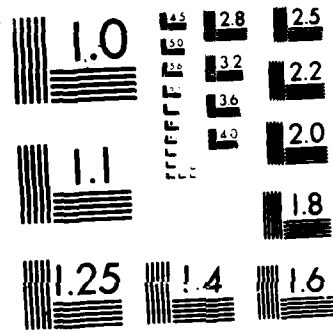
1/1

UNCLASSIFIED

F/G 21/9

NL





MICROCOPY RESOLUTION TEST CHART
NATIONAL BUREAU OF STANDARDS-1963-A

AD-A179 736

DTIC FILE COPY

12

AD

TECHNICAL REPORT BRL-TR-2780

ANNULAR LIQUID PROPELLANT JETS -
INJECTION, ATOMIZATION AND IGNITION

AVI BIRK
PHIL REEVES

MARCH 1987

STIC
ELECTE
APR 29 1987
S D
E

APPROVED FOR PUBLIC RELEASE, DISTRIBUTION UNLIMITED

US ARMY BALLISTIC RESEARCH LABORATORY
ABERDEEN PROVING GROUND, MARYLAND

20. ABSTRACT (CON'T)

Experiments are conducted: cold atomization and hot ignition. In the cold tests the LP and other liquids are injected into a room temperature argon gas. In the hot tests, LP is injected into the high pressure and temperature environment of steam and argon (22%,78%) obtained from prior combustion of oxygen-hydrogen-argon mixture in the chamber. Atomization is promoted when injecting with higher velocities into denser gas. Injection along a protruding center bolt promotes jet divergence; otherwise, jet convergence is observed. No particular standard atomization theory accounts for the observations. In particular, the predictions are poor for highly viscous liquids and injection into gas densities which are only an order of magnitude lower than the liquid density. The discharge coefficient of the thinner jets is low and highly influenced by the nozzle geometry. Jet ignition is difficult to achieve at pressures below 10 MPa. Partial decomposition of the LP is observed for lower pressures. The appearance of opaque brownish gas indicates NO_2 decomposition from the HAN component of the LP.

TABLE OF CONTENTS

	<u>Page</u>
LIST OF FIGURES.....	v
LIST OF TABLES.....	vii
I. INTRODUCTION.....	1
II. JET BREAK-UP ASPECTS.....	1
III. IGNITION CONSIDERATIONS.....	4
IV. EXPERIMENTAL.....	5
V. DISCUSSION OF RESULTS	
1. OPERATING CONDITIONS.....	8
2. DISCHARGE COEFFICIENTS.....	9
3. COLD ATOMIZATION TESTS.....	10
4. IGNITION TESTS.....	14
VI. CONCLUSIONS.....	21
REFERENCES.....	49
NOMENCLATURE.....	51
DISTRIBUTION LIST.....	53

Accession For	
NTIS GRA&I	<input checked="" type="checkbox"/>
DTIC TAB	<input type="checkbox"/>
Unannounced	<input type="checkbox"/>
Justification	
By _____	
Distribution/	
Availability Codes	
Dist	Avail and/or Special
A-1	



LIST OF FIGURES

<u>Figure</u>		<u>Page</u>
1	Functions f , X_m and Divergence Angle θ	27
2	Annular LP Injector.....	28
3	Pressure Regulation of Injector Gas Chambers.....	29
4	Injector Head Assembly.....	30
5	Experimental Set-up.....	31
6	Injection Measurements.....	32
7	Nozzle Configurations.....	33
8	Discharge Coefficients for LP 1846.....	34
9	Discharge Coefficients for Water and Ethanol.....	35
10	Injection into 1 atm Air, .005S Nozzle, $V=38$ m/s, $We_G < 10$, $K > 10$ (Left: Ethanol; Right: Water).....	36
11a	LP 1846 into 1 MPa Argon, .010S Nozzle, $V=60$ m/s, $We_G=456$, $K=5$	37
11b	Same as Fig. 11a but .010L Nozzle.....	37
12	LP 1846 into 5 MPa Argon, .010S Nozzle, $V=49$ m/s, $We_G=1559$, $K=0.76$	38
13	Injection into 5 MPa Argon, .005S Nozzle (Left: Water, $V=81$ m/s, $K=1.2$; Right: Ethanol, $V=78$ m/s, $K=0.82$).....	38
14	Jet Divergence Angles for .005L Nozzle.....	39
15	Injection into 5 MPa Argon, $We_G > 1350$ (Left: Water, .005L Nozzle, $V=68$ m/s, $K=1.26$; Right: LP 1846, .005LS Nozzle, $V=71$ m/s, $K=1.37$).....	40
16	Injection into 1.4 MPa Argon, $We_G > 850$, .005L Nozzle. (Left: Ethanol, $V=120$ m/s, $K=11.28$; Right: Water, $V=100$ m/s, $K=11.23$).....	40
17	Dow 550 Injection into 1.4 MPa Argon, $We_G=387$, .005L Nozzle. (Left: Before Injection; Right: $V=41$ m/s, $K=9.5$).....	41

LIST OF FIGURES (CON'T)

<u>Figure</u>	<u>Page</u>
18	Injection into 1.4 MPa Argon. $We_G > 380$, .005L Nozzle. (Left: LP 1846, $V=77$ m/s, $K=7.08$; Right: Dow 550, $V=41$ m/s, $K=9.5$).....41
19	Post Injection into 1.4 MPa Argon, .005L Nozzle. (Left: LP 1846; Right: Dow 550).....42
20a	Ignition Test 100C200I003S-a.....43
20b	Ignition Test 100C200I003S-b.....44
21a	Ignition Test 150C250I003S-a.....45
21b	Ignition Test 150C250I003S-b.....46
22	1846 LP into 5.5 MPa, 1800K, 22% Water, 78% Argon, $V=30$ m/s (Left: .001S Nozzle; Right: .003S Nozzle).....47
23	1846 LP into Figure 22 Environment. (Left: .002S7 Nozzle, $V=30$ m/s; Right: .005M15 Nozzle, $V=45$ m/s).....47
24	Figure 22 Environment (Left: Isooctane, .005S Nozzle, $V=45$ m/s; Right: LP 1846, .020S Nozzle, $V=20$ m/s).....48

LIST OF TABLES

<u>Table</u>		<u>Page</u>
1	Physical Properties of Injected Liquids.....	24
2	Operating Conditions With Regard To Atomization.....	24
3	Atomization Tests.....	25

I. INTRODUCTION

In recent years the development of a practical regenerative liquid propellant gun (RLPG) has been gaining momentum.¹ A key feature in the operation of the RLPG is that the liquid propellant (LP) burns as a spray. The experimental work reported here was prompted by the lack of information regarding RLPG type sprays. These sprays have unique geometries (annular) and occur in environments which are beyond those investigated today in other propulsion systems. Also, little is known about the ignition characteristics of LP sprays. In accordance with current RLPG injection geometry, an annular injection port is employed in this study. A previous study in BRL² investigated injection of LP from a circular orifice into open air. That study attempted to measure particle sizes for comparison with semi-empirical correlations found in the literature. Only partial success was achieved in the measurements and only in the dilute downstream region of the sprays. Agreement with theories was poor. The present study extends into much denser confined (and more practical) sprays where particle size distribution measurements are not feasible. Instead, global features of the sprays are studied. Jet break-up is studied in room temperature dense environment simulating RLPG gas densities. Jet ignition is studied in a less dense hot environment simulating RLPG ignition conditions. Most of the information gleaned in this study is from high speed photography using various fluids (Table 1). Other measurements yield discharge coefficients and ignition and combustion dynamics.

II. JET BREAK-UP ASPECTS

Injection velocities in an RLPG range from 50 m/s to 300 m/s in a 2000 K, 15 to 500 MPa environment. The jet gas Weber number ($We_G = \rho_G v^2 D / \sigma$) is greater than 40 and therefore aerodynamic forces are a major mechanism for jet breakup.³ This falls into the second wind induced regime, or into the full atomization regime, of primary jet breakup.⁴ In these regimes, the jet disintegrates into particles which are much smaller in diameter than the thickness of the annulus. The disintegration is the result of aerodynamic forces. Droplets form due to the growth of unstable short wavelength surface

waves caused by the relative motion of the jet and the ambient gas. Surface tension and viscosity impede the wave growth. In full atomization, jet breakup starts at the injection port exit as evidenced by its immediate divergence. Numerous studies in the past dealt with other mechanisms for full atomization, notably: jet turbulence, cavitation in the nozzle, boundary layer relaxation, and injection pressure oscillations. However, it is the aerodynamic theory which most successfully explains the experimental trends.^{4 5} Although the Reynolds number of the jet in the RLPG is well in the turbulence regime, the flow itself is only transitionally turbulent owing to the rather low L/D of the nozzle. Also, inherent to RLPG injection, the cavitation number ($K = (P_L - P_G)/(P_G - P_V)$) is less than 0.5, which is below the critical cavitation number for round orifices in steady flow.⁶ Cavitation may result in a two phase flow in the nozzle or in transition to turbulence. Cavitation is not entirely ruled out in the RLPG as the flow is transient and the geometry is rather different from a round straight orifice. The combustor in the RLPG is rather short; hence, the emphasis in this study is on the near field of spray, i.e., few jet diameter downstream of the injector.

The aerodynamic atomization theory which is considered here is Taylor's theory.⁷ It treats the primary atomization of the jet. The theory is valid for $\rho_G/\rho_L \ll 1$ and therefore applies best to the early ignition phase of the RLPG. The applicability of the theory to the later high pressure phase is questionable. The theory yields the jet divergence angle⁸ (Figure 1):

$$\tan \frac{\theta}{2} = A_1 \cdot \frac{\rho_G}{\rho_L}^{1/2} \cdot f\left(\frac{\rho_L}{\rho_G} B^2\right) \quad (1)$$

where $B = \frac{Re}{We} = \frac{\rho V D / \mu}{\rho V^2 D / \sigma} = \frac{\sigma}{\mu V}$

$A_1 = A_1(L/D, \text{ nozzle geometry})$ is an empirical constant. The function f (Fig. 1) assumes asymptotic behavior in two limiting cases:

case 1: for $\frac{\rho_L}{\rho_G} B^2 > 10$ $X_B = A_2 D \frac{\rho_L}{\rho_G}^{1/2}$ (2a)

$$\text{case 2: for } \frac{\rho_L}{\rho_G} B^2 < 0.1 \quad X_B = A_2 D \left(\frac{\rho_L}{\rho_G} B \right)^{1/3} \quad (2b)$$

where X_B is the full breakup length of the jet from its point of divergence and A_2 is a constant. Typically, $A_2 < 5$.

The theory⁷ yields also initial drop diameter d_p :

$$d_p = A_3 \frac{2\pi\sigma X_m}{\rho_G V^2} \quad A_3 \sim 1 \quad (3)$$

d_p is proportional to the wavelength of the most unstable wave (the dimensionless X_m). It decreases with increasing B (Fig. 1) which means that keeping all other parameters unchanged, larger droplets are obtained for higher viscosity. Note, that secondary atomization or coalescence may take place after initial jet breakup. In the RLPG, case 1 applies to the beginning of the ignition phase and case 2 applies to the high pressure phase (see Table 2). Firing RLPG on a very cold day may be entirely in the case 2 regime as the LP becomes highly viscous. If the parameter B is very small, the jet may not achieve complete breakup within the short confines of a typical RLPG combustor and the droplets may be larger. In experiments, only the divergence angle can be measured but not X_B . Most work reported today applies to case 1 conditions (e.g., diesel applications) and corroborate Taylor's theory for low ρ_G/ρ_L . As the density ratio becomes larger the jet divergence approaches an asymptotic value.

Considering the possibility of cavitation or of a fully turbulent jet, a turbulence theory may apply. The theory⁹ states that the jet behaves like a single phase turbulent jet injected into a lower density environment where it diffuses in a divergence angle of:

$$\tan \theta/2 = 0.13 (1 + \rho_G/\rho_L) \quad (4)$$

for $\rho_G/\rho_L \rightarrow 0$, $\theta/2 = 7.4$ degrees, and for $\rho_G/\rho_L = 0.3$ (e.g., RLPG), $\theta/2 = 9.6$ degrees. The jet velocity, viscosity, and surface tension bear no role and the dependence on the density ratio is not great. Inherently, the particle sizes are infinitesimally small.

In general, there is a dearth of information regarding the atomization characteristics and overall spray propagation of annular jets, particularly when bound to flow over a protruding center bolt for some distance downstream of the injector (the RLPG case). It is therefore an objective of the current study to shed light on the subject as well as to investigate the applicabilities of the two theories discussed in the previous paragraphs. This can be done by measuring d_p and $\theta/2$ for various conditions. In this study, only $\theta/2$ is measured.

III. IGNITION CONSIDERATIONS

The combustion characteristics of LP droplets in gun pressures are yet to be explored. Well into the combustion cycle, the environment is supercritical for the LP; hence, the droplets may turn into puffs of reactive gas before igniting. The present study considers only the subcritical conditions which exist during the ignition phase, i.e., pressures below 20 MPa. In ignition experiments¹⁰ of single droplets injected into the combustion products of atmospheric flame, the droplets were observed to microexplode with most of their volume intact. It was surmised that the microexplosion was due to the superheating of the water in LP. Before exploding, the droplet diameter decreases with time following the d_p^2 law (i.e., $d_p^2 \sim \tau$) and decomposition products other than water evolved from the droplet. However, the droplets (150 μm) involved and the ignition delays (80 msec) in atmospheric pressure are atypical of the ignition environment in the RLPG. The relative importance of the various time scales in droplet ignition shift according to droplet size and environment. The burn rate may depend on the droplet size and proximity of the flame to the droplet surface.¹¹ It may shift from the d_p^2 law to d_p to a lower power law. If microexplosion occurs, it may be induced by chemical reactions rather than by water superheating. In the present study attention is focused on the ignition of dense sprays. Here,

there is the added complexity of particle cloud dynamics and transport properties. The nature of the reactions leading to ignition: whether gas phase, heterogeneous, or liquid phase bear importance to the intensity of the ignition as well as to its delay. If the bulk of the spray ignites at once, undesired large pressure excursion results.

In the RLPG, the LP is injected into a 2000 K environment which is more than 70% (mole fraction) steam. Of interest are: a) how the jet breakup changes when injecting into high temperature environment, and b) what the operating conditions are to achieve prompt spray ignition, as LP ignition temperature may be environment dependent. In tests¹² where the LP is allowed to boil, ignition occurs at the boiling temperature of the solution as the water in the propellant (15-20%, which serves as solvent/moderator) is evaporated away. In other atmospheric tests where water evaporation is inhibited ignition per se did not occur at all. In these tests,¹³ the LP droplets which were immersed in heated immiscible host liquid reached temperatures over 230 C before exploding due to water superheating without indicating prior reactivity. In the RLPG, the high partial pressure of the steam will suppress the LP water evaporation, thus driving the spray temperature rather high before ignition. Current RLPG igniters are solid propellant based, but future ones may employ LP for gas generation. This means that even in the ignition phase, the jet will encounter a steam rich environment. In the ignition tests conducted in this study, the jet is injected into a 22% steam environment.

IV. EXPERIMENTAL

The experimental set-up and details of the major components are outlined in Figs. 2 to 7. It is basically an arrangement where an annular injector, which forms the base of a combustor, injects vertically into the combustor.

A skeletal outline of the injector is shown in Fig. 2. The injector is composed of two main sections connected by a pressure transmitting push-rod: the pressure generating gas chambers, and the injector head for the liquid injection. The two sections are further detailed in Figs. 3 and 4. The basic

injector gas chambers assembly was used in prior experiments.² However, the present work necessitated an order of magnitude higher LP injection mass flow rates (i.e., higher push-rod velocities). This was achieved by the pressure regulation scheme outlined in Fig. 3.

The principle of operation is as follows. Prior to injection the push-rod is pushed down to the base of chamber A and the stem valve seals the orifice between chambers A and B. The valve is held in place by the set screw. The injector is filled with LP (which is exposed to the combustor environment). Chamber B is pressurized with nitrogen and the set screw is recessed. The valve is held in place by the pressure in B. Injection is achieved by suddenly pressurizing chamber C. The stem valve is pulled back and the gas in B rushes into A. Pressure amplification is obtained on the top end of the push-rod due to its smaller area. The pressure is transmitted hydraulically to the LP via the transmission fluid (Dow 200 silicon fluid, 10 cs viscosity) and the floating piston which also seals the LP from the transmission fluid. Such an arrangement provides smooth flow in the LP chamber and enables the measurement (by a Kistler 601B) of the differential injection pressure ($P_L - P_G$). In preliminary tests, the pressure in the transmission fluid was found to be identical to the pressure in the LP. This was done by replacing the exchangeable bolt (Fig. 4) with a dedicated pressure transducer housing bolt and measuring both transmission fluid and LP pressures simultaneously. A comb-like mask is attached to the push-rod and its prongs pass through a photointerrupter (GE H11A2) as the push-rod is pushed (Fig. 5). The frequency of the modulated light is recorded and the rod velocity is calculated. The volume swept by the rod is the volume of LP injected. Knowing the nozzle port area, the injection velocity is easily calculated.

Plots of the injector's pressures and photointerrupter output are given in Fig. 6. They were taken off a digital wave recorder (Nicolet 4094) which is used to record all the data from the tests. Typically, the first 1 msec of the injection is transient due to inertias in the system. After stabilizing, a pressure amplification of about 8.5 is obtained across the push-rod. The peaks on the injection velocity indicator plot represent the mask prongs which are 3 mm apart.

The injector is capable of injecting up to 4 cc of LP in 3 to 20 msec at up to 30 MPa. Its annular nozzle geometry is variable. The various nozzle configurations used are shown in Fig. 7. The outside diameter of the nozzles is fixed at 19 mm (0.75"). Exchangeable cylindrical bolts with smaller diameters are threaded onto the injector to provide annulus thicknesses ranging from 0.0264 mm to 0.51 mm (0.001" to 0.020"). Some of the bolts protrude above the injector face to simulate the RLPG geometry. The liquid in the injector is exposed to the combustor gas prior to injection. The injected liquids and their physical properties are given in Table 1.

A coupler connects the combustor onto the injector (Fig. 5). The combustor is segmented to provide two test volumes. It is cylindrical inside with dimensions of 2.25"ID by 16"L (1050 cc), or 2.25" by 8"L. The combustor to jet aspect ratio is thus 3. For the ignition tests, the larger test volume was used to reduce heat losses and to provide more residence time for igniting the sprays. The combustor has four opposing rectangular sapphire windows with the dimensions: two at 3.875" by 1.375", and two at 2.750" by 0.750". The combustor is rated for 17 MPa. For the cold atomization tests it is pressurized with argon, nitrogen, or helium. For the hot ignition tests it is filled with stoichiometric mixture of $7\text{Ar}+2\text{H}_2+\text{O}_2$. The argon serves as a diluent to prevent detonation. Compared with another possible inert-diluent, helium, the argon renders the mixture denser and facilitates spark ignition. The mixture is ignited by a spark plug and the LP is then injected into the combustor. The transient pressure in the combustor is recorded; thus, enabling a calculation of the average gas temperature prior to injection. Typically, due to heat losses to the walls, only 80% of the theoretical adiabatic pressure is obtained.

Particle size measurements by light scattering methods are ruled out as the sprays under study are very dense and transient. Light obscuration by the sprays is close to 100% and their duration is less than 10 msec. Available particle sizers require better than 50% light transmission and an order of magnitude longer spray durations. Therefore, high speed photography is the tool of choice which reveals only the global dynamic structure of the sprays. High speed movies were taken routinely using a Photec camera. An EG&G strobe (2 μsec pulse) or a copper vapor laser (10 Watt, Oxford Laser, 20 nsec

pulse) synchronized by the camera, provide back lighting for the photography. Typically, the camera was run at 5000 frames per second using a Kodak VNF 7240 film. The camera initiated a timer-sequencer which sequences all operations with a 1 ms time resolution. A comprehensive flow diagram of the test controls and data acquisition is provided in Fig. 5.

V. DISCUSSION OF RESULTS

1. OPERATING CONDITIONS

The range of operating conditions covered in the experiments, with implication to atomization, is given in Table 2 where it is compared to those calculated from the data of an experimental 30-mm RLPG. In the table, the numbers for the RLPG correlate vertically (e.g., for 2.8 msec, $V=300$ m/s and $Re=178000$). The numbers for the injector tests are a compendium of over 80 tests with LP 1846, water, ethanol, and Dow 550 liquid. The higher Reynolds number tests correspond to water which is seven times less viscous than the LP. The lower Re tests correspond to the 550 liquid which is 17 times more viscous than the LP. The injector tests simulate the ignition phase of the RLPG (represented by the 0.2 msec numbers). The cold tests cover density ratios well within the high pressure phase of the RLPG (the 2.8 msec). This is achieved by injecting the LP into room temperature argon. Argon has almost twice the molecular weight of the RLPG combustion products. The tests relate to the transition between case 1 to case 2, and to case 2 of the aerodynamic theory of jet breakup discussed before (see also Fig. 1).

Most tests were conducted with the 005 nozzles. The gap size (.005") is large enough for eccentricity effects to be small and it provides longer and steadier injections than the larger gap nozzles. Injection mass flow rates were up to 1.5 kg/sec which is 1/10 of the 30-mm RLPG. They are two orders of magnitude higher than typical diesel injectors.

With respect to turbulence,¹⁴ the parameters of importance are Re and L/D . Although the flow can be turbulent for $Re>2300$, it takes some distance to transit to turbulence. In the absence of cavitation, the transition will

occur at $L/D \sim 10^5/Re$ and fully developed turbulence will occur at $L/D > 40$. The nozzle flow in the 30-mm RLPG is laminar during ignition and only marginally turbulent later. In most of the injector tests the flow is laminar. In tests where the cavitation number, K , is greater than 1, the flow may be turbulent. It is of interest to see if, for the suspected turbulent flows, the jet divergence corresponds to the turbulent jet theory.

2. DISCHARGE COEFFICIENTS

A by-product of the tests is the discharge coefficient C_D . It was calculated for the straight nozzles (Table 3) and averaged from the flatter segment of the injection pressure curves. The standard definition of C_D is given in Fig. 8 where it is shown versus $Re^{1/2}$ for protruding (005L, 005LS, 010L) and non protruding nozzles (005S, 005SS, 010S). Although the number of tests conducted is not statistically representative, general trends are nevertheless apparent. Within the range tested, C_D increases with Re for all the nozzles with $K > 1$. However, for the smaller gap nozzles 005, C_D drops when transitting from $K < 1$ to $K > 1$, a possible indication of the onset of cavitation. This trend is very apparent in Fig. 9. For the larger gap 010 nozzles, C_D is insensitive to K .

For the same Re , the C_D for the shorter nozzles 005SS and 005LS is higher than for longer 005S and 005L nozzles. This is not suprising since the shorter nozzles have smaller viscous friction loss. A look at this loss is warranted:

For a steady laminar viscous flow between long coaxial cylinders of radii r_1 and r_2 ($r_2 > r_1$), the drop in pressure due to friction is given by:¹⁵

$$P = \frac{8 \mu L V}{r_1^2 \left(n^2 + 1 - \frac{n^2 - 1}{\ln n} \right)} \quad n = r_2/r_1 \quad (5)$$

Equation 5 holds for $L/D > 200$, when the velocity profile is fully developed. It can be seen that P will be enhanced for $D/2 = (r_2 - r_1) \ll r_1$ and

increasing μ and V . Since LP is rather viscous (especially when very cold), large pressure gradients are required to achieve high initial injection velocity, V , when the opening gap, D , is still small. In this case L/D is still large, the flow is laminar, and Eq. 5 holds. It means that C_D will be rather small at the initiation of the LP injection in the RLPG. As an illustrative example: a 005S nozzle of the present study injecting LP at $V=100$ m/s will experience a drop of 482 psi due to friction (Eq. 5). Ideally ($C_D = 1$), 100 m/s is generated by a drop of 750 psi. Therefore, the calculated C_D will be $(750/(750+482))^{1/2} = 0.78$. Since L/D for the 005 nozzle is only 25, the friction loss will be smaller than that indicated by Eq. 5. The loss is obviously smaller for the shorter 005SS nozzle, for which $C_D = 0.87$. The same calculation for a smaller gap 002S nozzle yields $C_D = 0.48$, a dramatic decrease in C_D .

Another interesting trend is that C_D for a protruding nozzle is smaller than for the nonprotruding one. This is pronounced for the 005 nozzles (Figs. 8, 9). For the larger gap 010 nozzle the trend is less apparent.

In Fig. 9, the C_D values are generally below those in Fig. 8. Possibly it is due to turbulence as the Re numbers in Fig. 9 are much higher than in Fig. 8. From experiments with small round orifice nozzles,¹⁶ it is known that the C_D dependence on Re is rather complex.

In conclusion, barring nonsteadiness effects, C_D is expected to be low, erratic, and sensitive to nozzle geometry at the opening of the injection port gap in the RLPG. As the gap widens, C_D should increase more smoothly toward the ideal value of 1. Thus, the C_D trends are more important for the ignition phase of the RLPG.

3. COLD ATOMIZATION TESTS

a. General. The jet breakup tests are summarized in Table 3 and Figs. 10 to 19. The water and the LP sprays are almost indistinguishable (the water disperses somewhat better). The ethanol sprays disperse much better and appear more finely atomized. This can be predicted from Eq. 3, since ethanol has a surface tension which is about 1/3 of water. Another possible manifes-

tation of Eq. 3 is the effect of high viscosity. The highly viscous Dow 550 liquid disperses more poorly than the LP, although its surface tension is similar to ethanol. A peculiar behavior of the 550 liquid is its fogging of the combustor chamber volume when pressurized. Apparently, the pressurized chamber gas dissolves into the 550 liquid. The slight pressure fluctuations during the chamber gas loading liberates excess gas from the liquid. This disrupts the liquid-gas interface which, due to its low surface tension, generates fog. To eliminate fogging (which impedes photography), a thin insulating layer of lighter and immiscible water was floated on top of the 550 liquid.

b. The Structure of Annular Jets. Injection into low pressure environment is depicted in Fig. 10. Strictly based on their We_G number, the jets are not in the atomization regime. However, their cavitation numbers are above critical, which may cause atomization. The water jet rolls into capillary strings but does not atomize. In contrast, the ethanol atomizes well, as also indicated by its divergence at the nozzle's exit. Both jets converge downstream, an indication of a pressure imbalance between the outer and inner surfaces of the hollow jets. A possible reason for the convergence is the evacuation of the gas, enveloped by the jet, by entrainment with the moving inner jet surface. Cavitation is stronger in ethanol which has higher vapor pressure than water. Also, the We_G for ethanol is higher than that of the water due to its lower surface tension and it is more susceptible to cavitation induced atomization.

The gas density in Figs. 11a, b (tests 31, 32 in Table 3) approaches that which is provided by the igniter in the RLPG. The jets depicted are in the atomization regime. Although cavitation may exist ($K = 5$), based on Fig. 10-right ($K > 5$) it should not by itself atomize the LP which is similar to water in surface tension. The atomization here is primarily aerodynamic. Equation 3 indicates a primary drop size $d_p = 20 \mu\text{m}$ which is below the resolution of the film. The jet from the nonprotruding nozzle converges (Fig. 11a); the jet from the protruding one diverges (Fig. 11b). Light transmission through the bottom of the Fig. 11a jet indicates a short intact liquid core, an indication of the second induced regime of atomization. The subsequent convergence of the jet is peculiar to annular jets which are not bound to flow over inner

walls. Redivergence occurs further downstream as the jet's annular core reaches a minimum. The predictions of Taylor's theory⁷ are suspect in this case. Unbound annular jets belong to the ignition phase of the RLPG. As the center bolt in the RLPG protrudes, the geometry resembles Fig 11b. The jet diverges on the center bolt. If it is fully atomized on the bolt, pressure balance can be maintained across the jet's wall by turbulent gas diffusion through the droplets. In the tests conducted, convergence of the jet downstream of the bolt is still observed for bolts shorter than 1.5 times the annulus diameter. The significance of the annulus diameter with respect to the jet hydrodynamics is not established in this work. The experimental setup precludes varying the diameter.

Figure 12 (test 21 in Table 3) depicts a jet emanating from the same nozzle of Fig. 11a, but into a 5 times denser gas. As before, the jet converges but redivergence starts sooner with mushrooming of the jet's tip. This is an indication of complete atomization and retardation of the droplets by the dense gas drag. The movies reveal recirculation of the gas in the chamber which has an ID only 3 times the jet diameter. This is enhanced for a shorter chamber. Recirculation entrains droplets in a vortex like motion. Residence time of the droplets, before impingement on the walls, is enhanced which is beneficial in a combustion environment.

The lateral symmetry of the jet is retained for longer distance if the jet's momentum with respect to the gas it interacts with is higher. For smaller gap nozzles, the momentum is lower (lower mass flow rate) and the jet loses symmetry upon atomization and interaction with the recirculating gas flow. (In a combustion environment, this may lead to flame fluctuations). Figure 13 is such an example. The ethanol in Fig. 13-right (test 39 in Table 3), owing to its lower density and velocity has smaller momentum than the water in Fig. 13-left (test 35). The ethanol jet collapses laterally while the water jet retains its symmetry. Flow over a center bolt will prevent the lateral collapse of a jet.

c. Divergence Angles. Divergence angles are measured (averaged from 5 movie frames) only for flows over center bolts and with an uncertainty of 1 degree. The divergence is larger for the smaller gap nozzles. For the 0101

nozzle, the angles vary between $\theta/2 = 4$ to 7 degrees for LP injection into 1 to 10 MPa argon; for the 005L nozzle, they vary between 3 to 9 degrees. In both cases, the angles reach asymptotic value at around 10 MPa, which corresponds to $\rho_L/\rho_G = 8.5$. For a particular nozzle gap $D/2$, changing the length L (e.g., 005L nozzle versus 005LS) did not make much difference.

The data obtained for the 010 nozzle are too scant to be plotted. The data obtained for the 005 nozzle (Fig. 14) were somewhat more precise (as steadier and longer injection are obtained for the smaller gap nozzle) and extensive. Although, the data are rather scattered, careful study reveals some general trends. If the aerodynamic theory of atomization holds for the entire range of the tests; then, according to Eq. 1 all the points should fall on a straight line (the slope of which is empirical) - which is not the case. The theoretical line in Fig. 14 is chosen somewhat arbitrarily to pass between the points which have the lowest cavitation number K for any particular chamber pressure P_G (to rule out cavitation effects). It is apparent that for any given liquid and P_G , an increase in injection velocity V results in a wider divergence angle $\theta/2$. This behavior does not fit the theory. Also, the data for Eq. 2b conditions which are represented by the 550 liquid, do not fit the theory. (For the 550 liquid in Fig. 14, K has little meaning since it entails the large pressure gradient due to viscosity alone.) The overall trend of the data is for $\theta/2$ to reach asymptotic value for the higher ρ_G/ρ_L where the theory is less precise. Such a trend was found in the past for tests with round orifices.⁴ In the few tests (for $\rho_G \ll \rho_L$) where the argon is replaced by the same pressure helium (i.e., lower density), the jet hydrodynamics is similar to the one observed in the corresponding density lower pressure argon; which is in agreement with the aerodynamic theory of atomization.

The water and ethanol jets in Fig. 14 are turbulent; their $\theta/2$ is in the range of 7 to 10 degrees which may be in agreement with the turbulent jet theory (Eq. 4). The data obtained are too scant to prove it. The photographic appearance of the jets does not yield any clues. For example, in Fig. 15, the LP and water jets look rather similar, but the water jet is turbulent ($Re = 17127$, test 34 in Table 3) and the LP is not ($Re = 3611$, test 17). In Fig. 16, the ethanol jet is turbulent ($Re = 22182$, test 42) but its $\theta/2$ is

well above Eq. 4 prediction. The LP jet is probably turbulent ($Re = 5116$ and $K = 11.23$, test 27) but its divergence is well below the one predicted from Eq. 4. Nevertheless, the turbulent theory may apply better for lower ρ_L/ρ_G , i.e., for higher P_G .

The atomization mechanism of the high viscosity 550 liquid seems to be different from the lower viscosity liquids. The pictures depicted in Figs. 17 to 19 are of the jet boundary. Despite its low surface tension, the 550 liquid surface rolls into detached thin ligaments (Fig. 17, test 50 in Table 3). Only then, droplets are pinched from the ligaments, perhaps due to surface tension driven instabilities. In Fig. 18, the boundary of an LP jet (test 29) is shown for comparison. Here, small droplets detach directly from the boundary, an indication of aerodynamic driven instability. The picture in Fig. 18-right was taken 0.2 msec subsequently to the one in Fig. 17-right. The pictures in Fig. 19 were taken after the completion of the injection. Note the difference in particle sizes. The more viscous 550 droplets are much larger than the higher surface tension LP droplets.

In summary: the predictions from the aerodynamic theory may be valid for the lower ρ_G/ρ_L conditions during the ignition phase of the RLPG (as long as the annular jet flows over a center bolt) but not later in the combustion cycle; then, the turbulent theory may apply. The theories are poor for high viscosity liquids (e.g., very cold LP).

4. IGNITION TESTS

a. General. Although the steam-argon gas provides a clear environment for photography, difficulties were encountered for pressures above 6 MPa due to intense background radiation from contaminants in the chamber. The LP flame, which is yellowishly faint, fades into such a background. Therefore, most of the tests were conducted around 5.5 MPa and 1800 K, obtained (after some cooling) from the combustion of 10_2+2H_2+7Ar at 1 MPa. At pressures above 6 MPa, the LP occasionally ignited in the injector, prior to injection, by contact with the hot gas. A 7 degree tapered nozzle (S7 in Fig. 7) which is opened by the injection pressure, was constructed to seal the injection port from the hot gas prior to injection. In tests conducted at 13 MPa and 2000 K,

the LP jet was observed (albeit with difficulty) to ignite and burn completely within the field of view. This was accompanied by a sharp rise in the combustor pressure. In accordance with nozzle geometry of the ignition phase in the RLPG, most ignition tests were conducted with the nonprotruding center bolt nozzles. The tests shown in Figs. 20 to 24 represent the minimum pressures and temperatures in which ignition was observed in this work. For these conditions, the hydrodynamics of the jets resemble the one in the equivalent density cold tests (i.e., 1 MPa argon). The resemblance is not surprising since, for moderate pressures, most of the heat transfer to the jet takes place only after atomization is completed and droplet-gas mixing is enhanced.

b. Ignition Dynamics from Pressure Traces. Much information regarding the LP spray ignition characteristics can be gleaned from Figures 20a,b and 21a,b. These figures are the recorded pressure traces of the tests in which LP 1846 is injected from a 003S nozzle into the combustion products of 100 psi (Fig. 20a,b) and 150 psi (Fig. 21a,b) H_2 , O_2 , Ar gas mixture. Both P_G and P_L are recorded simultaneously. (Although the liquid is continually exposed to the combustor gas, the liquid pressure measurement (P_L) is most accurate during the injection period when the floating piston and push-rod (Fig. 4) are in motion. By finely tuning the spacing between the floating piston and the pressure transducer, a better agreement between P_G and P_L is achieved for the entire test duration.)

The various points of significance are marked on the pressure traces as follow. Point 0 denotes the initial conditions of the reactive cold $1H_2 + 2O_2 + 7Ar$ mixture in the combustor, and LP in the injector. Point 1 denotes the spark ignition of the mixture. Point 2 denotes the completion of the reaction to yield $2H_2O + 7Ar$. The adiabatic values calculated using the NASA Lewis thermodynamic code¹⁷ are shown for comparison. Heat losses to the combustor walls result in a P_G drop, a subject which is discussed later. Points 3 and 4 denote the LP injection period. Points 6 and 7 are local minimum and maximum on the P_G curve which denote the LP spray ignition and its combustion completion. Points 5 and 8 are on the extrapolated P_G curve (i.e., P_G as recorded in separate tests without LP jet injection) and correspond to times

t_6 and t_7 respectively. Note, the repeatability of the P_G curves in Figures 20a and 20b and in Figs. 21a and 21b.

A discussion of the combustion of the gas mixture (O_2 , H_2 , Ar) in the combustor follows. Although the laminar flame velocity of the mixture is below 3 m/s, the flame propagation in the combustor reaches 30 m/s (as evidenced from the time between points 1 and 2, t_{12} , and also from photography). It is because the flame propagates here in a closed tube where pressure compression waves precede the flame to ever increase the temperature of the yet unreacted mixture. The flame accelerates and the flow behind it turns somewhat turbulent. The convective heat losses to the walls result in a marked chamber pressure drop especially during flame propagation. Later, the losses taper off. Heat transfer considerations and some photographic evidence suggest that not much of the steam (the combustion product) condenses on the walls during the test time (100 msec). Therefore, it is assumed that for each 10 moles of the reactants ($1H_2 + 2O_2 + 7Ar$), 9 moles of products ($2H_2O + 7Ar$) are obtained. Owing to the constant volume of the combustor, the gas temperature T_G (prior to LP ignition) may be simply calculated as follows:

$$T_G = 10/9 (P_G T_O/P_O) \quad (6)$$

T_G comprises the right ordinates in Figs. 20 and 21. Although strictly from thermodynamic considerations,¹⁸ T_G is not uniform along the combustor, the variations are small and are rapidly dissipated by the flame induced turbulent gas motion in the chamber. The gas motion decays rapidly and it is small compared to the LP injection velocities (as photography reveals that the LP sprays are not distorted by the gas motion in the chamber). For long duration jets, the P_G drop due to heat losses results in the later portion of the jet being injected into markedly colder environment. This is a shortcoming of the experiment but not a critical one.

Obviously, upon injection heat is transferred from the combustor gas to the sprays. A too excessive steep drop in T_G due to spray heating is not

desired in the tests. The following rudimentary heat transfer calculations will show that the combustor gas has ample heat capacity to provide for the spray heating to ignition. The calculations are for the conditions of Fig. 21a (which is also pictorially shown in Fig. 22). Assuming that the entire spray is injected at t_6 ($P_G = 5.5$ MPa, $T_G = 1800$ K), the partial pressure of the steam is approximately 1.2 MPa for which the saturation temperature is $T_L = 463$ K. The LP will reach this temperature (if not yet ignited) before any water evaporates from it. The combustor contains $m_G = 13.8$ g of hot gas with about 7010 calories ($= m_G C_{V_G}(T_6 - T_L)$, $C_{V_G} = 0.38$ cal/g-K from Ref. 17) available to heat the injected LP ($m_L = 3$ g injected at $T_0 = 298$ K) to T_L . The LP requires 282 calories ($= m_L C_{p_L}(T_L - T_0)$, $C_{p_L} = 0.57$ cal/g-K) to reach T_L . Therefore, for the following calculations, the combustor gas temperature gradient between the chamber gas and the liquid is assumed constant.

It is worthwhile to estimate the time scale of droplet heating. Following a single primary detached droplet from the jet boundary, the time t_h for inert heat-up to T_L is:¹⁹

$$t_h \sim (\rho_L C_{p_L} d_p^2 T_L) / (12 K_G h/h_{Re=0} (T_6 - T_L)) \quad (7)$$

where $h/h_{Re=0} = 1 + 0.278 Re_G^{1/2} Pr_G^{1/3}$

A characteristic time for droplet slow down, t_m , due to drag is estimated from a balance of drag and inertial forces on the droplet:¹⁹

$$t_m = (4 \rho_L d_p) / (3 \rho_G C_d v) \quad (8)$$

where $C_d = 0.27 Re_G^{.217}$ (drag coefficient)

The liquid sheet thickness from the 003S nozzle is $76 \mu\text{m}$; therefore, droplet sizes should be no greater than $76 \mu\text{m}$. Also, as approximated by Eq. 3, $d_p = 72 \mu\text{m}$. Conservatively, substituting $d_p = 76$ ($\text{Re}_G = 936$) in Eq. 7, one obtains (for $\text{Pr}_G = 0.7$, $K_G = 0.000257 \text{ cal/cm-K-s}$): $h/h_{\text{Re} = 0} = 8.6$. Then, $t_h = 0.56 \text{ msec}$ (for a droplet moving at the injection velocity) and $t_{h(\text{Re} = 0)} = 4.8 \text{ msec}$ (for a droplet at rest). The calculation for t_m yields $t_m = 0.21 \text{ msec}$ which is of the order of t_h and indicates that the droplet slows down considerably while being heated up. Therefore, t_h will assume an intermediate value, around 2.5 msec , during which the droplet will travel about 75 mm (still within the field of view to be observed whether igniting).

Similar calculations for the lower pressure conditions in Fig. 20a still yield similar t_h . Therefore, if the LP droplet ignites readily when reaching a temperature when significant water evaporation commences, then the sprays in Figures 20a,b should have ignited within the injection duration t_{34} and be observed so photographically. However, this is not the case. The pressure traces in Figures 20a,b suggest a too large heat transfer to the LP spray prior to LP ignition. To estimate the spray temperature T_{L6} at t_6 , the following thermal balance may be written:

$$m_G C_{vG} (T_5 - T_6) = m_L C_{pL} (T_{L6} - T_0) \quad (9)$$

In Eq. 9 it is assumed that the spray is well mixed with the ambient gas. In both Figures 20a and 20b, $T_5 - T_6$ is about 166 K . Also, $m_L = 3 \text{ g}$, $m_G = 9.22 \text{ g}$. Eq. 9 yields $T_6 = 638 \text{ K}$ which is rather high for ignition (as it is well above the boiling temperature of the LP). In addition, T_6 is only an average temperature; according to calculations (Eq. 7), many primary droplets should reach much higher temperatures at T_6 . While T_{L6} is the same in both Fig. 20a and fig. 20b, for the higher P_6 in Fig. 20b, the ignition is faster and more intense than in Fig. 20a. This indicates clearly that LP ignition depends on pressure as well as on temperature. In practice, the spray partially decomposes before reaching the above calculated T_{L6} but little heat is released. The decomposition products reach the temperature T_6 which is well above the leftover liquid at T_{L6} . Eventually exothermic reactions take place between the diffused decomposition products and the liquid.

The assignment of ignition delays to sprays based on pressure data is somewhat arbitrary. Without photography one can not determine spatial and temporal history of the portion of the spray which ignites first. If the ignition delay is too long, the spray tip may pool on the end wall of the chamber and partially decompose there. This is of particular importance in an RLPG configuration where the combustion chamber length is very short initially. A short ignition delay is desired in the RLPG as otherwise the jet may reach the cold end walls terminating the combustion cycle or promoting hang-fire situation. Defining in Figures 20a,b and 21a,b the ignition delay as $t_6 - t_3$, then delays of 12 and 14 msec are obtained for Figures 20a and 20b respectively (during which the sprays are already off the view windows). In contrast, in the higher pressure tests of Figures 21a,b, the spray ignites more readily, within the injection duration ($t_6 < t_4$) and within the photographic view. Ignition delays of 5 and 6 msec are obtained for Figures 21a and 21b, respectively.

To estimate how much LP is consumed (in Fig. 21) during t_{67} , m_{LG} , the following equations may be written:

$$P_7 V_G = (m_{LS}/M_{LG} + m_G/M_G) R T_7 \quad (10)$$

$$m_{LG} C_{V_{LG}} (T_F - T_7) = m_G C_{V_G} (T_7 - T_8) \quad (11)$$

Eq. 10 is the equation of state, and Eq. 11 is a heat balance. $T_F = 2570$ K is the flame temperature of the LP 1846. $C_{V_{LG}} = 0.4$ cal/g-K, $C_{V_G} = 0.38$ cal/g-K, $M_{LG} = 22.8$ gmole, $M_G = 34.7$ gmole, $m_G = 13.8$ g. The unknowns are T_7 and m_{LG} .

After algebraic manipulation, a quadratic equation is obtained for T_7 which yields:

For Fig. 21a: $T_7 = 1677$ K, $m_{LG} = 1.5$ g

For Fig. 21b: $T_7 = 1943$ K, $m_{LG} = 1.5$ g.

The approximate calculations above indicate that despite their different ignition pressures P_6 , in both Figures 21a and 21b, about 50% of the LP mass reacted to completion and in similar combustion times. However, as already mentioned, ignition delay was shorter in the higher pressure test of Fig. 21b. Besides pressures and temperatures, the degrees of spray atomization and propagation (i.e., particle sizes and hydrodynamics) have bearing both on the ignition delays and combustion times. Different nozzles produce different sprays which have different ignition and combustion characteristics. Although, the ignition delays in Figures 21a,b are rather short, the long combustion times are not practical for the ignition phase of an RLPG. It is conceivable that for the same combustor conditions of Figures 21a,b other nozzle geometries will result in much shorter combustion times as well as ignition delays.

c. Ignition Dynamics from Photography. The ignition phenomena of LP sprays issuing from different nozzle configuration are depicted in Figs. 22 to 24.

In Fig. 22-left, the spray is dilute and there is little interaction between the droplets; partial ignition is observed, possibly of the smaller droplets. In Fig. 22-right, where the spray is much denser, partial decomposition (but no flame) is observed of clusters of droplets. This is evidenced by the irregular tufted appearance of the jet in its diverging region (i.e., after atomization). Partial decomposition liberates opaque NO_2 from the propellant. Fig. 22-right is the pictorial representation of Fig. 21a. For this case, ignition occurs downstream of the view window. Only about 50% of the LP burns to completion. The balance is apparently partially decomposed, primarily from the tufted jet boundaries.

The divergent tapered nozzle in Fig. 23-left issues a conical jet which does not converge. (Tests with wider gap nozzles result in jet convergence despite the tapering). Since the liquid sheet thickness here is only 25 μm , the droplets are small enough to heat up in less than a millisecond to temperature well over 500 K; nevertheless, the spray is not fully ignited and consumed while in the field of view. Instead, partial decomposition and regions of ignition are observed. In Fig. 23-right the jet is thicker. As

the jet flows over the divergent center bolt, it slows, thins, and breaks into cluster of droplets. Heat transfer to the diluted spray is enhanced which results in spotted ignition. Some droplets hit the walls where they partially decompose. In this configuration, the penetration distance of the spray down the combustor is limited.

Figure 24-right shows a slow thick jet with a mushroomed tip of atomized droplet cloud. The better mixing and longer residence times of the cloud facilitates its ignition. The intense localized heat release results in combustion times of less than 1 msec, well within the field of view.

Figure 24-left is shown to prove the heat transfer estimates given before. Isooctane is injected into environment which is supercritical for it (same environment as Fig. 22-right). The supercritical conditions for isooctane are: $P_{cr} = 2.58$ MPa and $T_{cr} = 544$ K. The isooctane which is a pure fuel cannot react with the inert combustor gas. It is observed to flash immediately into gas upon injection. (The gas pyrolyzes and later, after cooling, forms soot.) This is an indication that the heat transfer is indeed high, enough to bring the liquid to temperature above 544 K in less than a millisecond. As already seen, such temperatures are not sufficient to ignite the LP in a similar time duration. The LP requires pressures above 10 MPa to ignite that readily.

In summary: for Figs. 22 to 24 conditions, calculations indicate that the droplets should reach at least 463 K while in the field of view. Nevertheless, ignition was not always observed. The small droplets in the dilute sprays ignite, but they do not support flame propagation through the entire spray. It is conceivable that the ignition temperature is well above 463 K in a steam rich environment. Also, the chemical induction times may depend on the chemical composition of the environment around the droplets.

VI. CONCLUSIONS

The present study touched upon a wide range of RLPG type spray physics. Although, for practical reasons, the study is cursory in some areas, it

nevertheless identifies areas which warrant further study. The study covered test conditions in which precise quantification of data is not feasible. Future studies should concentrate deeper on identifying and quantifying the physio-chemical mechanisms of LP droplet ignition and combustion. Also, worth pursuing is the sizing of droplets obtained from primary atomization. The followings are the conclusions and recommendations of this study:

1. LP jets at room temperature atomize readily in gun conditions.
2. The near field atomization characteristics of annular sprays are too complex to be fully accounted for by the standard aerodynamic theory (which is applied for diesels) or by the turbulent jet theory. In particular:
 - a) If not injected along a protruding center bolt, annular jets converge prior to divergence.
 - b) The aerodynamic theory predictions of liquid jet divergence in a dense gas are poor when the gas density is higher than one tenth of the liquid density. For such high gas densities, the turbulent divergence theory may apply provided that the liquid is clearly turbulent.
 - c) More research is needed with thicker, higher velocity jets (i.e., higher Re number jets) injected into denser gases, to assess the applicability of the turbulent jet theory to gun conditions. Unfortunately, this will be very difficult to achieve in laboratory experiments.
 - d) The atomization characteristics of cold LPs which are more than 10 times viscous than usual are peculiar and have to be studied further. Very high viscosity clearly impedes atomization. The implications are mostly for the ignition phase of the RLPG.
3. The discharge coefficients of thin (<0.25 mm) annular jets are low and highly dependent on the nozzle geometry. The discharge coefficients of thicker jets are less dependent on the geometry and are more predictable.

Therefore, if marginal igniters are used in the RLPG, careful consideration should be given to the discharge coefficient behavior during nozzle opening.

4. The ignition temperature of LP droplets depends on the composition of the adjacent environment. In particular:
 - a) The LP does not ignite readily (in less than 2 msec) at pressures below 10 MPa. Between 5 and 10 MPa, the ignition depends highly on the spray particle size and velocity distribution.
 - b) The combustion mechanism of LP droplets have not been identified in the present work. Future work should address this subject in the 5 to 100 MPa pressure range, and for gas environments from 100% inert to 70% steam, 30% inert. At the higher pressures the droplets may burn supercritically as puffs of gas. The present test fixture is inadequate for this task.
5. Once the combustion times of LP droplets are known, they will be incorporated in the gun codes. Based on the results from the codes it will be determined if particle size distribution indeed affect gun performance and is therefore important.

Table 1. Physical Properties of Injected Liquids

	LP 1846	Water	Ethanol	Silicon Fluid Dow 550
Density $\frac{g}{cm^3}$	1.44	1	0.79	1.07
Viscosity $\frac{g}{cm-sec}$	0.071	0.01	0.0108	1.25
Surface Tension $\frac{g}{sec^2}$	66.9	72	24.1	24.5

Table 2. Operating Conditions With Regard To Atomization

	Single Firing	Annular Injector Tests	
	30mm RLPG 0.2 to 2.8 msec	Cold	Hot
V m/s	70 - 300	25 - 120	15 - 45
Re	19000 - 178000	60 - 25000	1000 - 10000
$\frac{\rho_L}{\rho_G} B^2$	1.24 - 0.0054	13 - 0.0001	10 - 2
$\left(\frac{\rho_L}{\rho_G}\right)^{\frac{1}{2}}$	8.74 - 2.70	30 - 2.91	30 - 7.14
L/D	5.54 - 2.89	6.25 - 125	6.25 - 125
K	< 0.5	0.2 - 13	0.2 - 5

Table 3. Atomization Tests

Liquid	Test*	P_{L-G}, MPa	C_D	$V, \text{m/s}$	Re_L	We_L	$\frac{\rho_L}{\rho_G} B^2 \left(\frac{\rho_L}{\rho_G}\right)^{1/2}$	$\left(\frac{\rho_L}{\rho_G}\right)^{1/3}$	K	$\frac{\theta}{2}$
1. LP 1846	1500A1000I005L	10.67	0.672	82.6	4226	37041	0.111	2.915	1.045	9
2.	1500A500I005S	4.32	0.712	55.5	3123	18395	0.245	3.685	0.423	
3.	1500A500I005M	6.51	0.601	57.5	2942	17950	0.228	3.729	0.638	5
4.	1500A500I005L	5.56	0.653	57.9	2962	18200	0.225	3.737	0.545	5
5.	1500A1000I010S	5.10	0.756	64.3	6579	44892	0.182	3.870	0.499	
6.	1500A1000I010M	5.01	0.778	65.6	6712	46726	0.175	3.896	0.491	
7.	1500A1000I010L	5.27	0.741	64.0	6548	44474	0.184	3.864	0.517	7
8.	1500A500I010S	2.21	0.646	36.2	3704	14229	0.576	3.196	0.217	
9.	1500A500I010L	2.65	0.661	40.5	4144	17810	0.460	3.318	0.260	5
10.	750A1000I005S	13.89	0.680	95.1	4865	49100	0.167	4.122	2.723	
11.	750A1000I005SS	11.82	0.785	101.3	5182	55711	0.147	5.674	2.317	
12.	750A1000I005L	14.05	0.676	95.1	4863	49048	0.167	5.555	2.755	5
13.	750A1000I005LS	12.82	0.770	103.4	5290	58044	0.141	5.713	2.512	5
14.	750A500I005S	5.67	0.675	60.5	3405	21859	0.412	4.778	1.111	
15.	750A500I005L	6.93	0.636	63.1	3228	21616	0.379	4.846	1.359	5
16.	750A500I005SS	6.47	0.729	69.6	3561	26299	0.311	5.007	1.268	
17.	750A500I005LS	7.00	0.710	70.6	3611	27045	0.303	5.030	1.373	5
18.	750A1000I010S	6.32	0.750	71.0	7264	54735	0.299	5.040	1.239	
19.	750A1000I010M	6.39	0.748	71.2	7285	55044	0.298	5.045	1.253	6
20.	750A1000I010L	6.36	0.742	70.5	7213	53967	0.304	5.028	1.247	5
21.	750A500I010S	3.88	0.666	49.4	5054	26497	0.618	4.466	0.761	
22.	750A500I010L	3.41	0.684	47.5	4860	24498	0.669	4.408	0.668	5
23.	750A500I010LS	3.70	0.640	46.2	4727	23176	0.707	4.367	0.725	6
24.	750A1000I020S	2.73	0.666	41.1	8472	37220	0.880	4.211	0.535	
25.	750A500I020S	1.89	0.547	28.3	5791	17392	1.884	3.709	0.371	
26.	750A500I020L	1.74	0.568	28.2	5771	17269	1.897	3.705	0.341	
27.	200A1000I005L	15.29	0.682	100.0	5116	54290	0.566	7.982	11.230	3
28.	200A500I010SS	3.98	0.760	56.9	5822	35154	1.748	7.270	2.925	
29.	200A500I005L	9.63	0.670	77.4	3960	32524	0.944	8.059	7.080	
30.	200A500I010LS	4.65	0.680	55.3	5658	33205	1.850	7.200	3.420	2
31.	150A500I010S	5.11	0.701	59.7	6108	38699	2.117	8.135	5.007	
32.	150A500I010L	5.40	0.690	60.4	6180	39612	2.068	8.166	5.293	4
33. Water	750A500I005S	4.30	0.230	77.1	21392	22906	10.290	3.435	2.329	0.843
34.	750A500I005L	6.43	0.595	67.9	17127	16150	13.270	2.233	1.260	7
35.	750A500I005S	6.25	0.721	81.2	20482	23097	9.279	2.369	1.225	

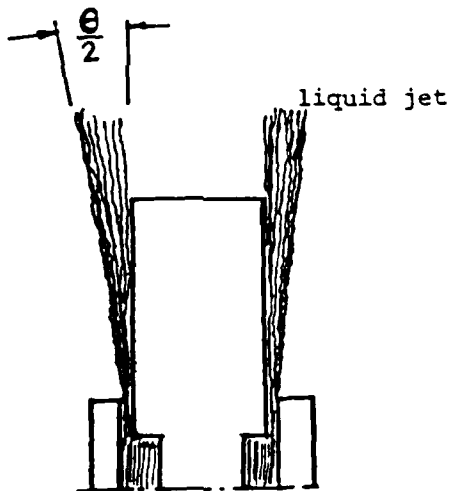
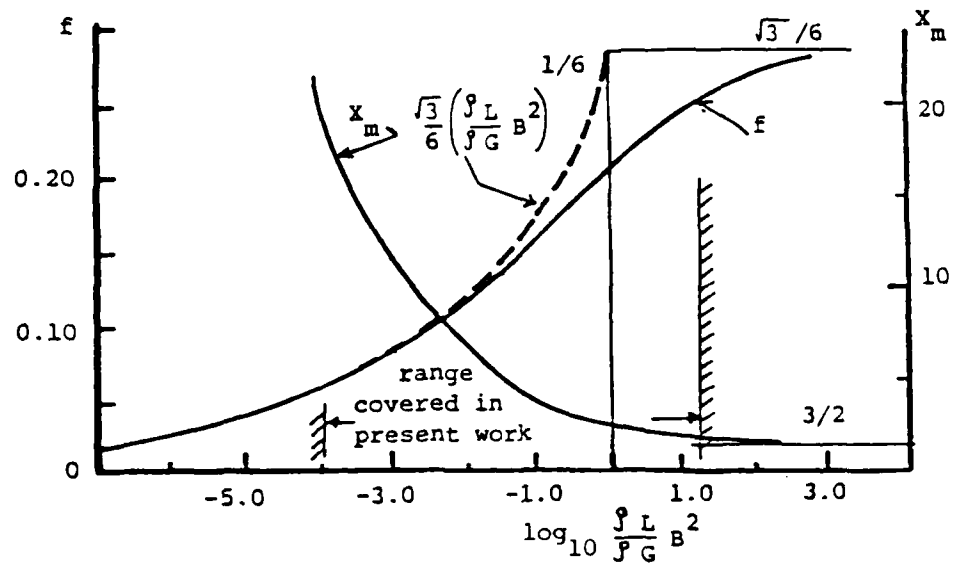


Figure 1. Functions f , X_m and Divergence Angle θ

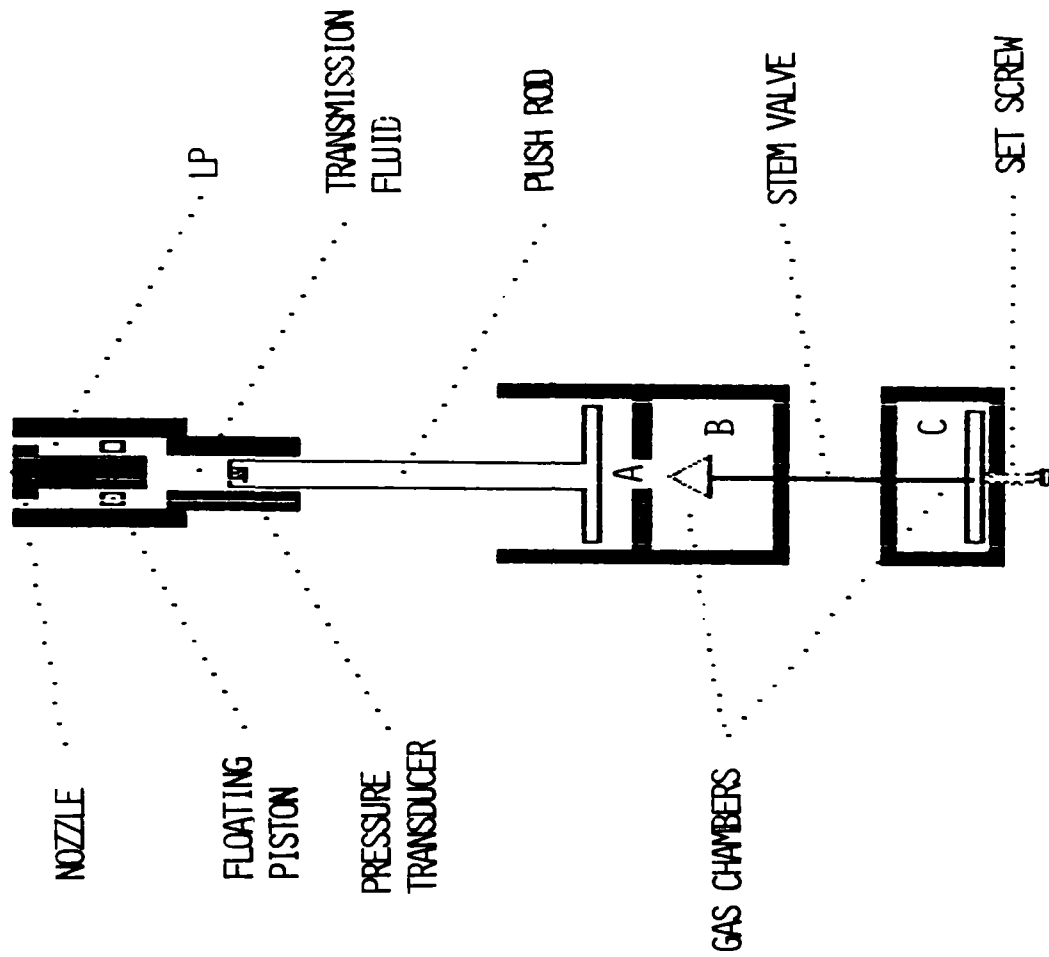
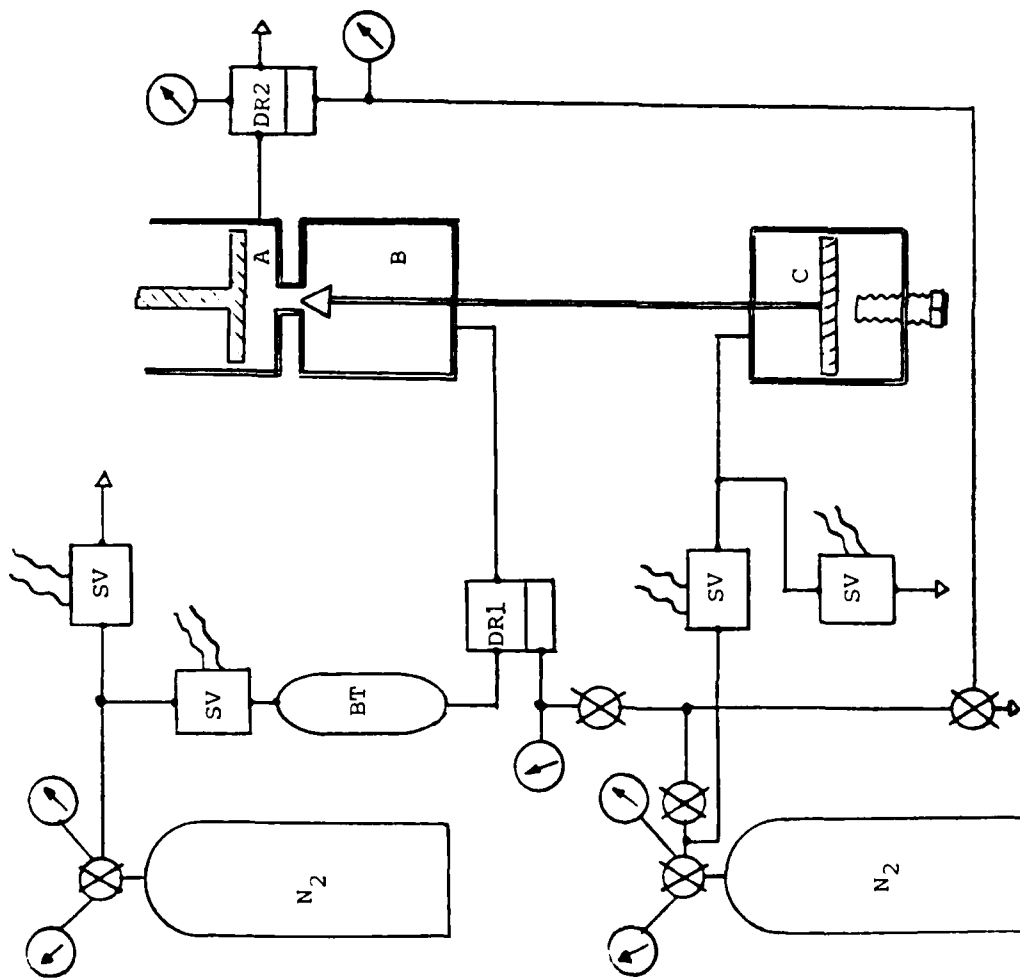


Figure 2. Annular LP Injector



SV Solenoid valve

BT Ballast tank to enable high mass flow rate.

DR1 Dome regulator to maintain preset pressure in B.

DR2 Dome regulator to keep the pressure in A below a preset maximum.

Figure 3. Pressure Regulation of Injector Gas Chambers

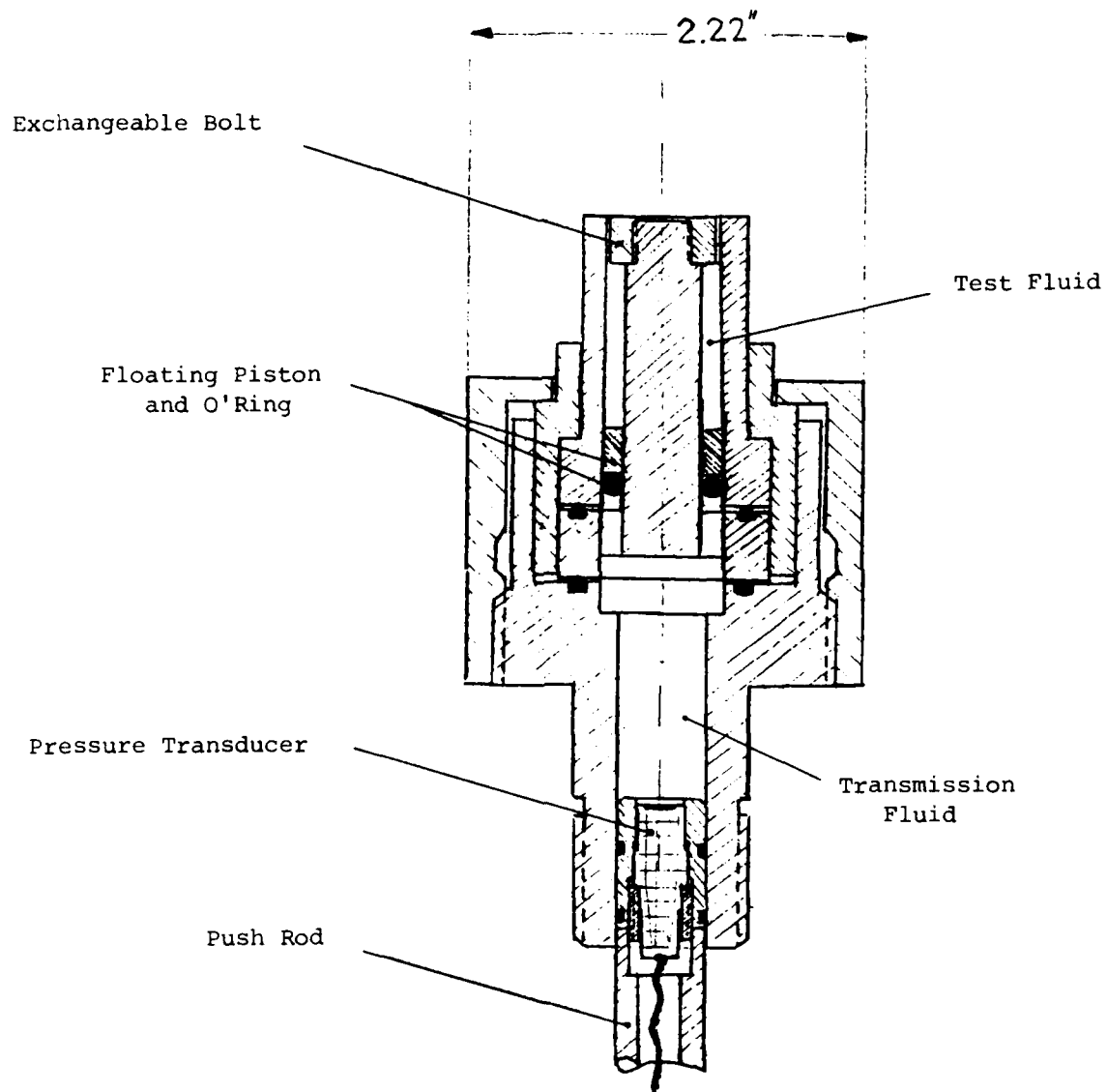


Figure 4. Injector Head Assembly

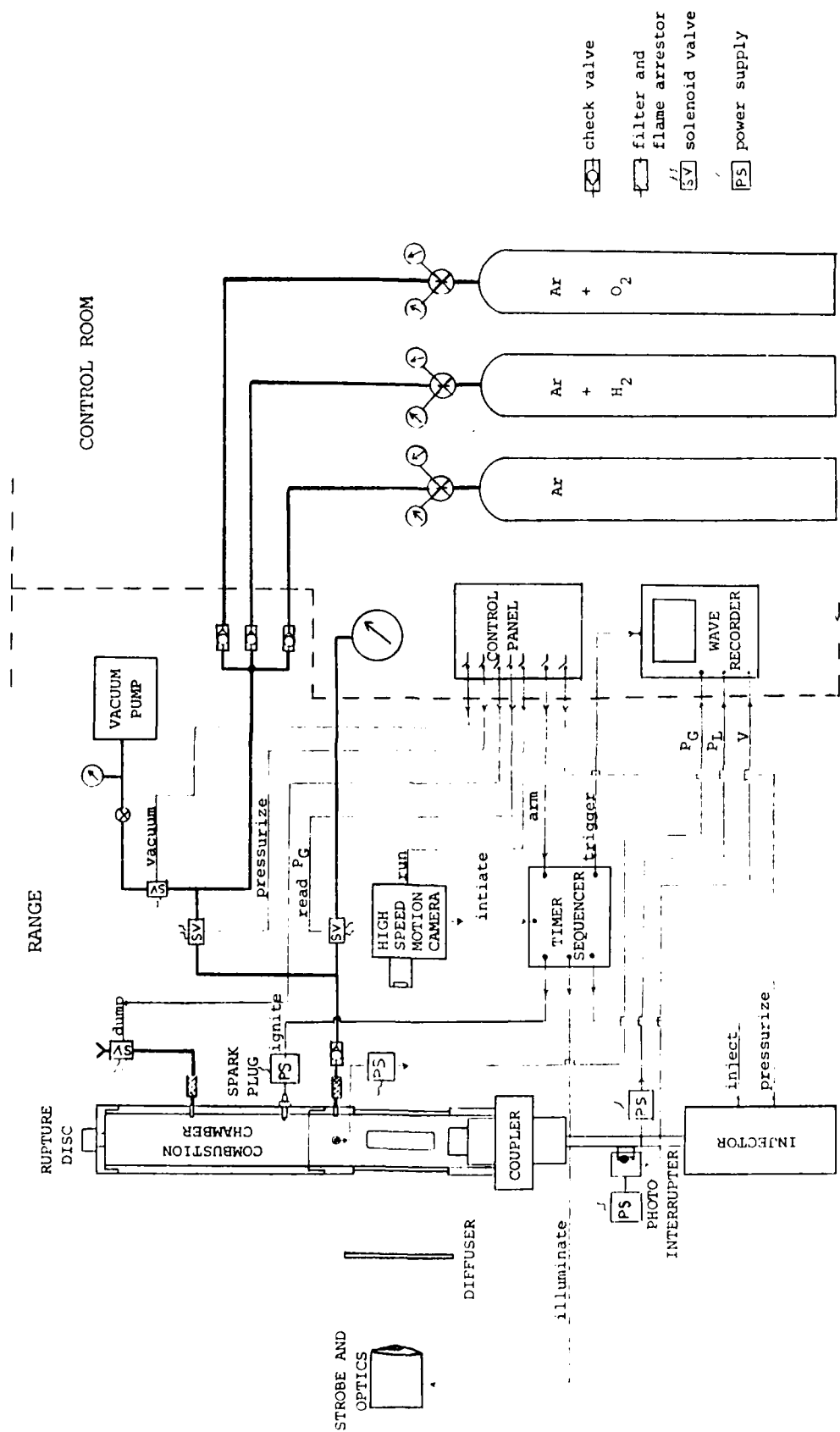


Figure 5. Experimental Set-up

750A 970I .005L 6/26/85

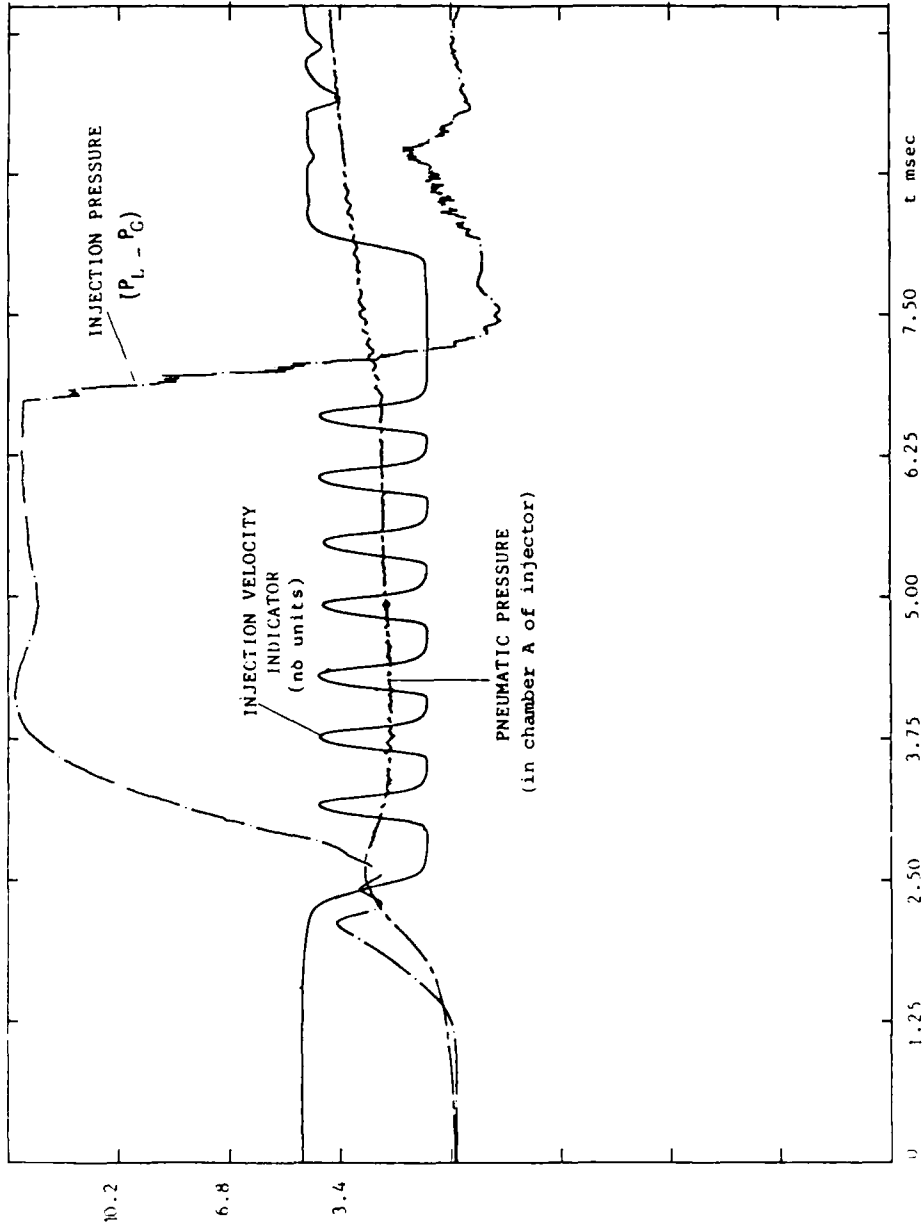
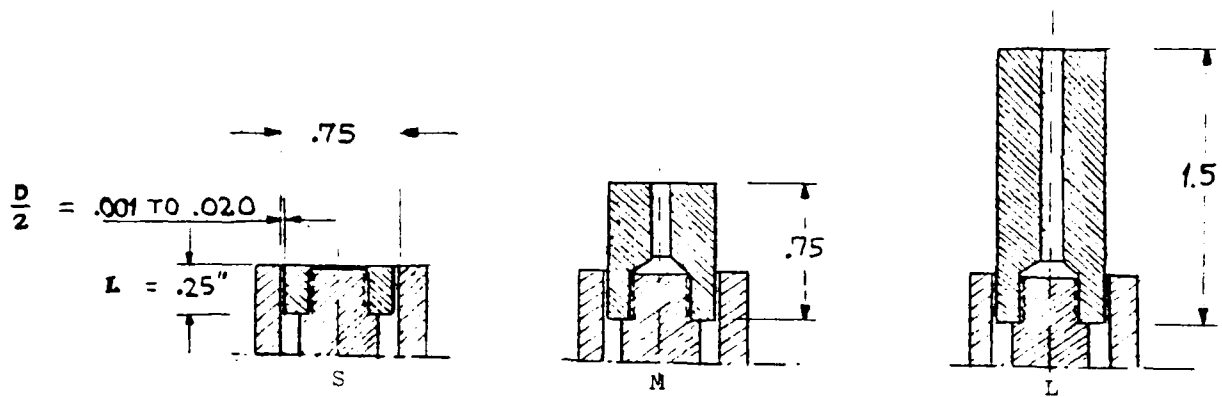


Figure 6. Injection Measurements



Nozzle Designation

For example: if $\frac{D}{2} = .005''$,
then above nozzle is 005S.

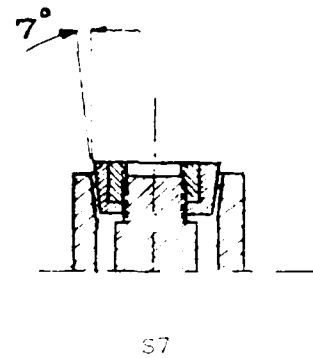
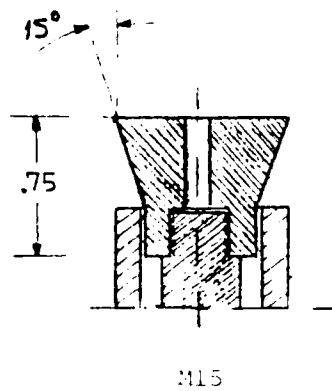
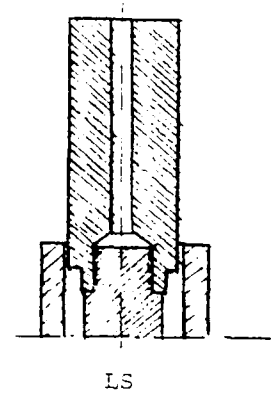
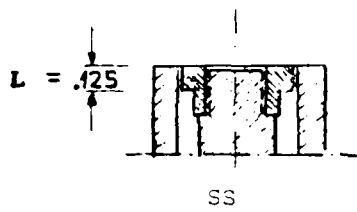


Figure 7. Nozzle Configurations

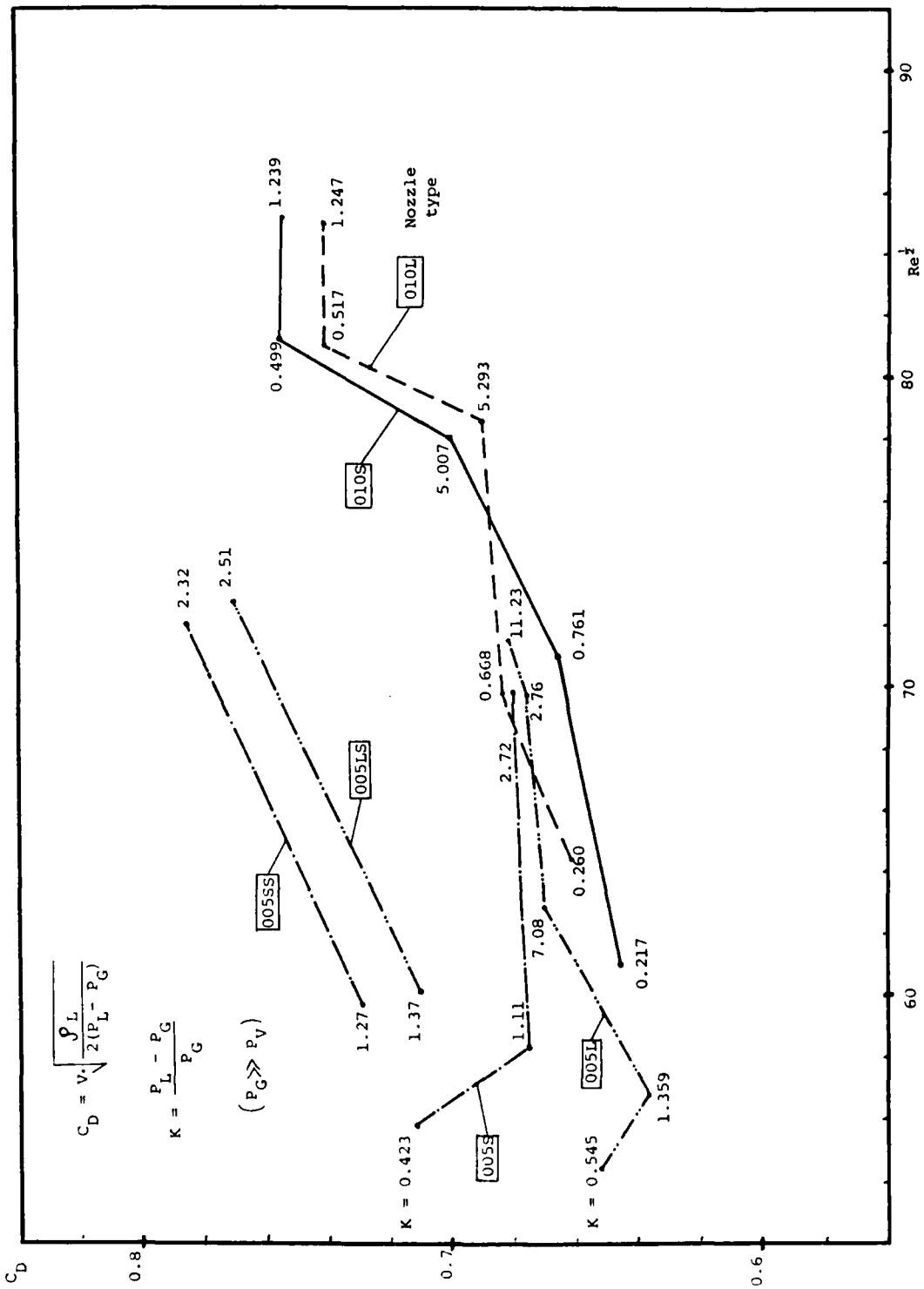


Figure 8. Discharge Coefficients for LP 1846

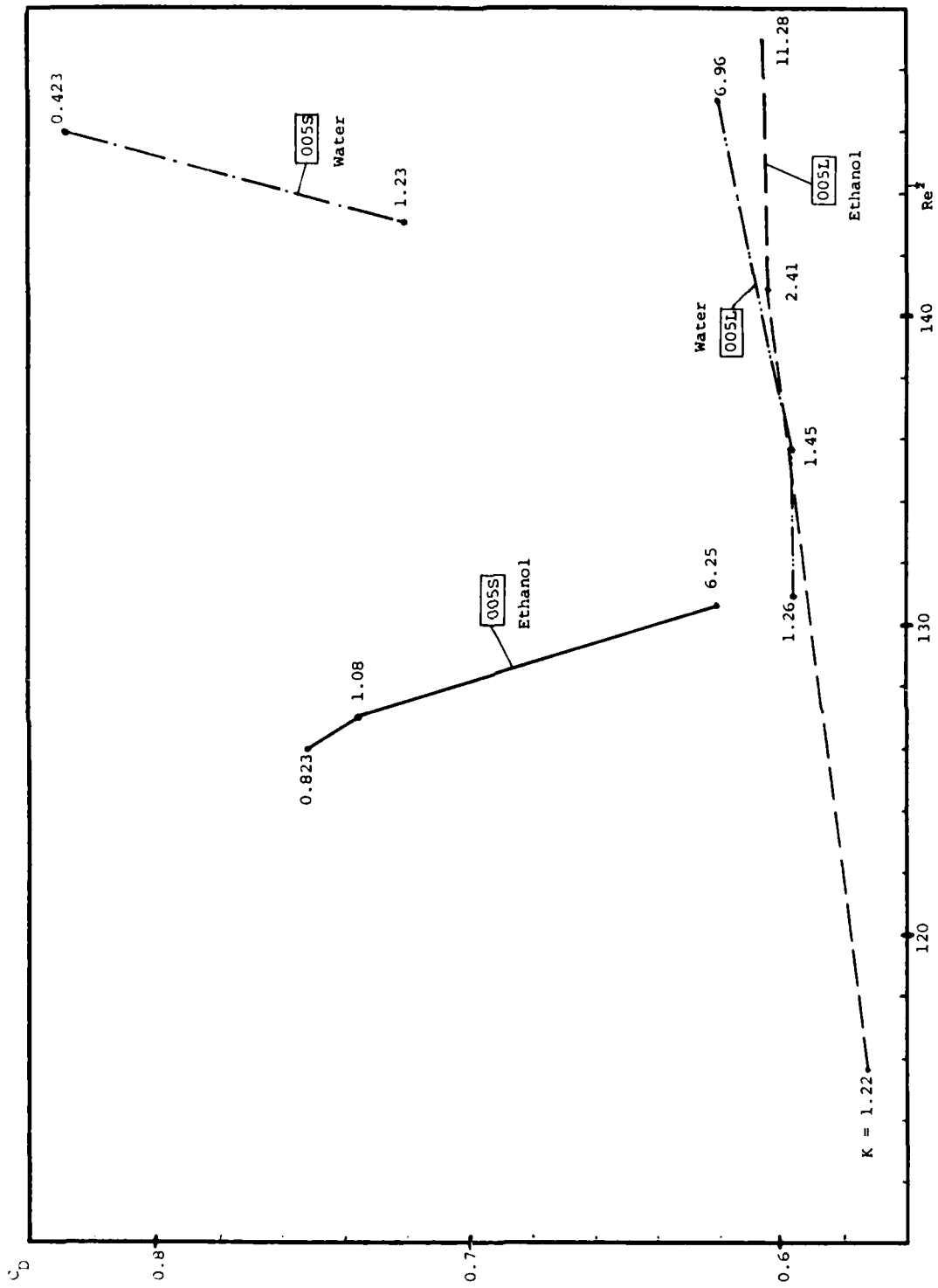
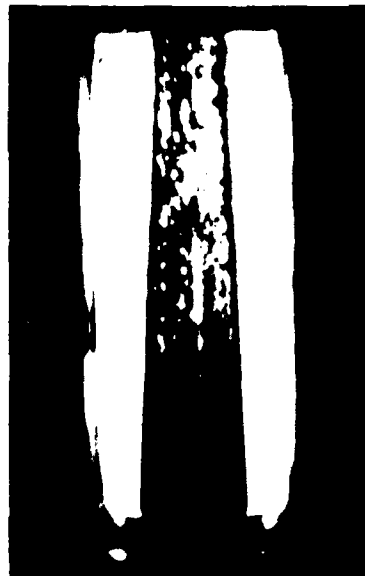


Figure 9. Discharge Coefficients for Water and Ethanol



Left: Ethanol
Right: Water

* EG&G Strobe

|←25 mm→|

Figure 10. Injection into 1 atm Air, .005S Nozzle,
 $V=38$ m/s, $We_G < 10$, $K > 10$

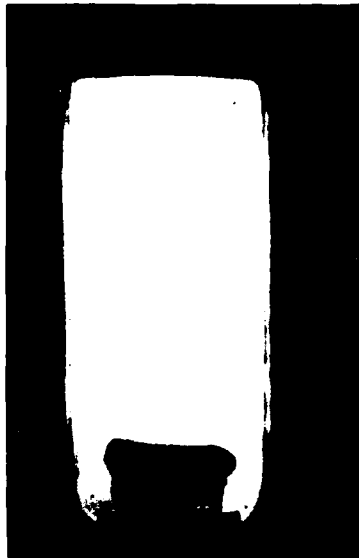


Left: $t < 1$ msec
Right: $t > 2$ msec

Figure 11a. LP 1846 into 1 MPa Argon, .010S Nozzle
 $V=60$ m/s, $We_G=456$, $K=5$



Figure 11b. Same as Figure 11a but .010L Nozzle.



Left: $t < 0.5$ msec
Right: $t \sim 1.5$ msec

Figure 12. LP 1846 into 5 MPa Argon, .010S Nozzle,
 $V=49$ m/s, $We_G=1559$, $K=0.76$



Left: Water, $V=81$ m/s
 $K=1.2$
Right: Ethanol,
 $V=78$ m/s
 $K=0.82$

Figure 13. Injection into 5 MPa Argon, .005S Nozzle

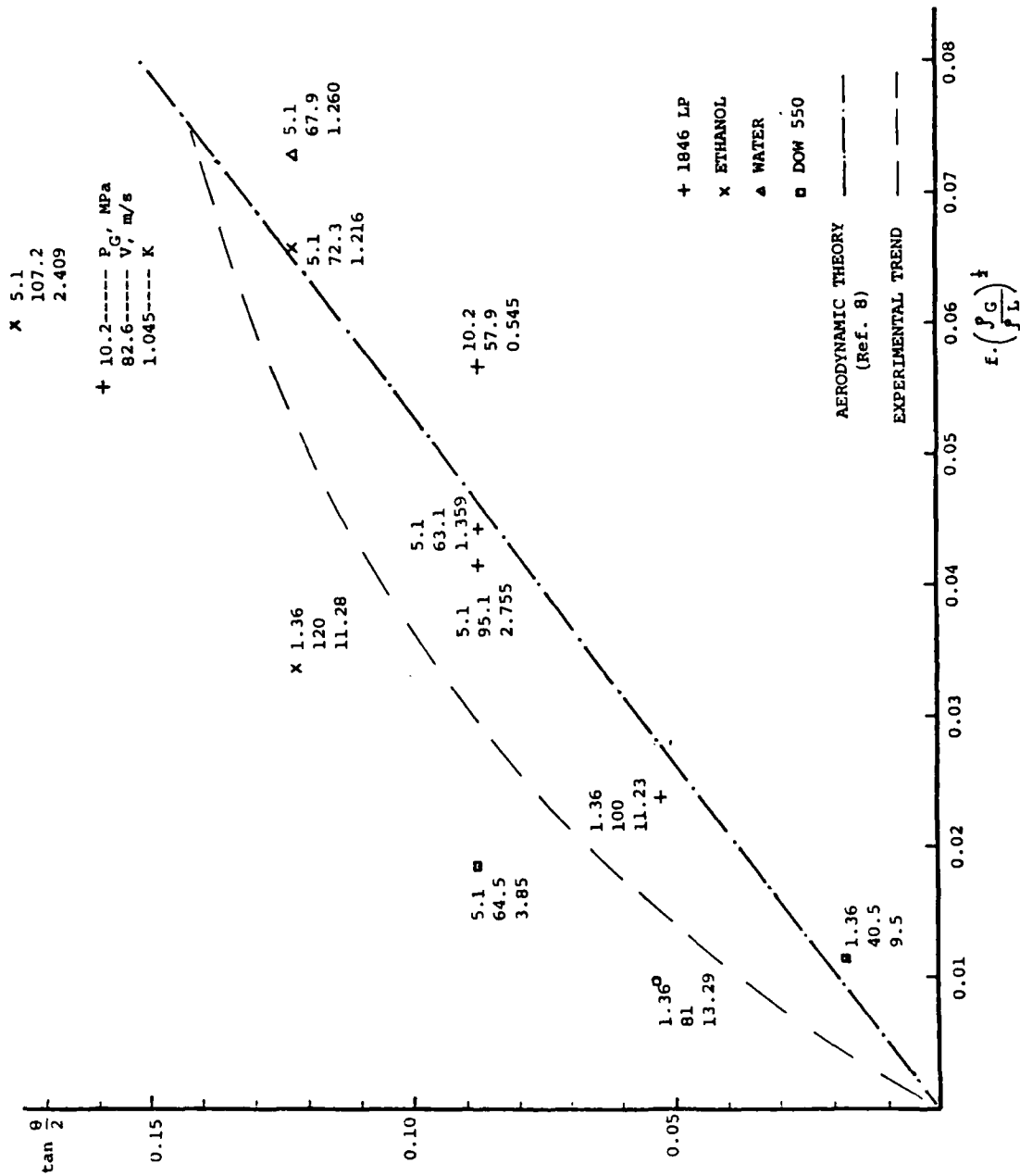
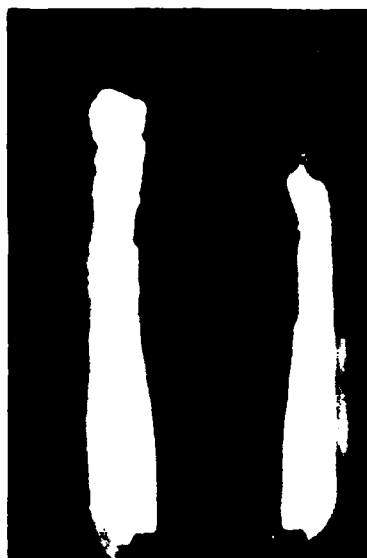
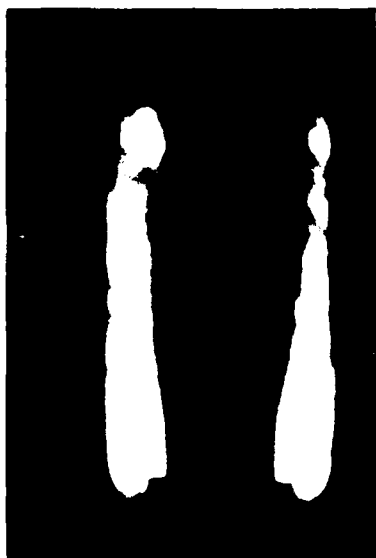
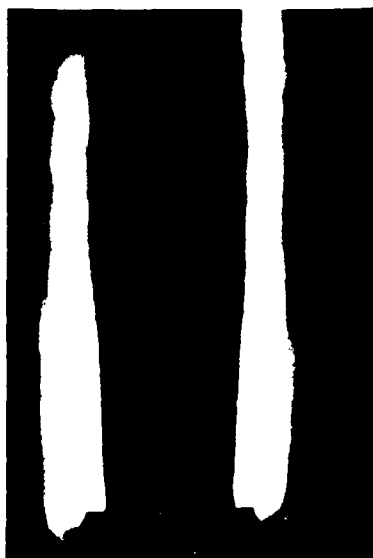


Figure 14. Jet Divergence Angles for .005L Nozzle



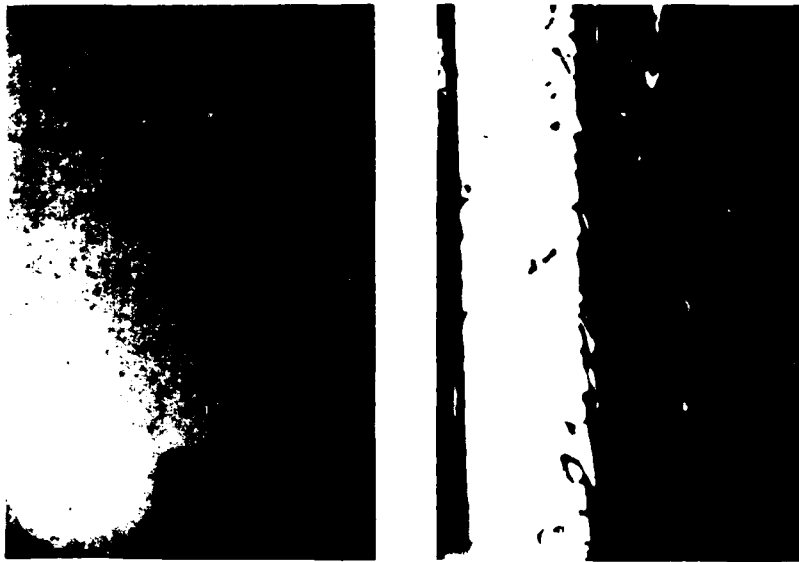
Left: Water, .005L
Nozzle, V=68 m/s
K=1.26
Right: LP 1846, .005LS
Nozzle, V=71 m/s
K=1.37

Figure 15. Injection into 5 MPa Argon, $We_G > 1350$



Left: Ethanol,
V=120 m/s
K=11.28
Right: Water,
V=100 m/s
K=11.23

Figure 16. Injection into 1.4 MPa Argon, $We_G > 850$, .005L Nozzle.



Left: Before Injection
(the tip of the
center bolt)

Right: $V=41$ m/s
 $K=9.5$

* copper vapor laser strobe

+ | 3 mm | +

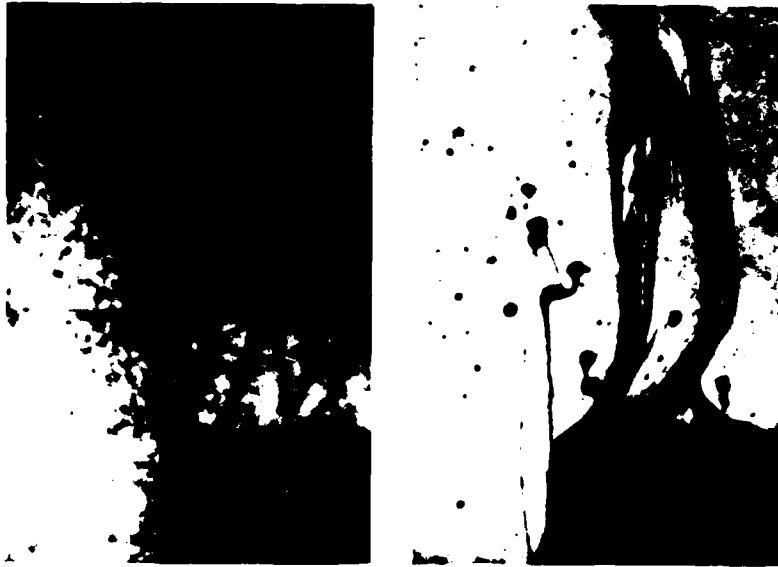
Figure 17. Dow 550 Injection into 1.4 MPa Argon,
 $We_G=384$, .005L Nozzle.



Left: LP 1846,
 $V=77$ m/s
 $K=7.08$

Right: Dow 550,
 $V=41$ m/s
 $K=9.5$

Figure 18. Injection into 1.4 MPa Argon,
 $We_G>380$, .005L Nozzle.



Left: LP 1846
Right: Dow 550

Figure 19. Post Injection into 1.4 MPa Argon,
.005L Nozzle.

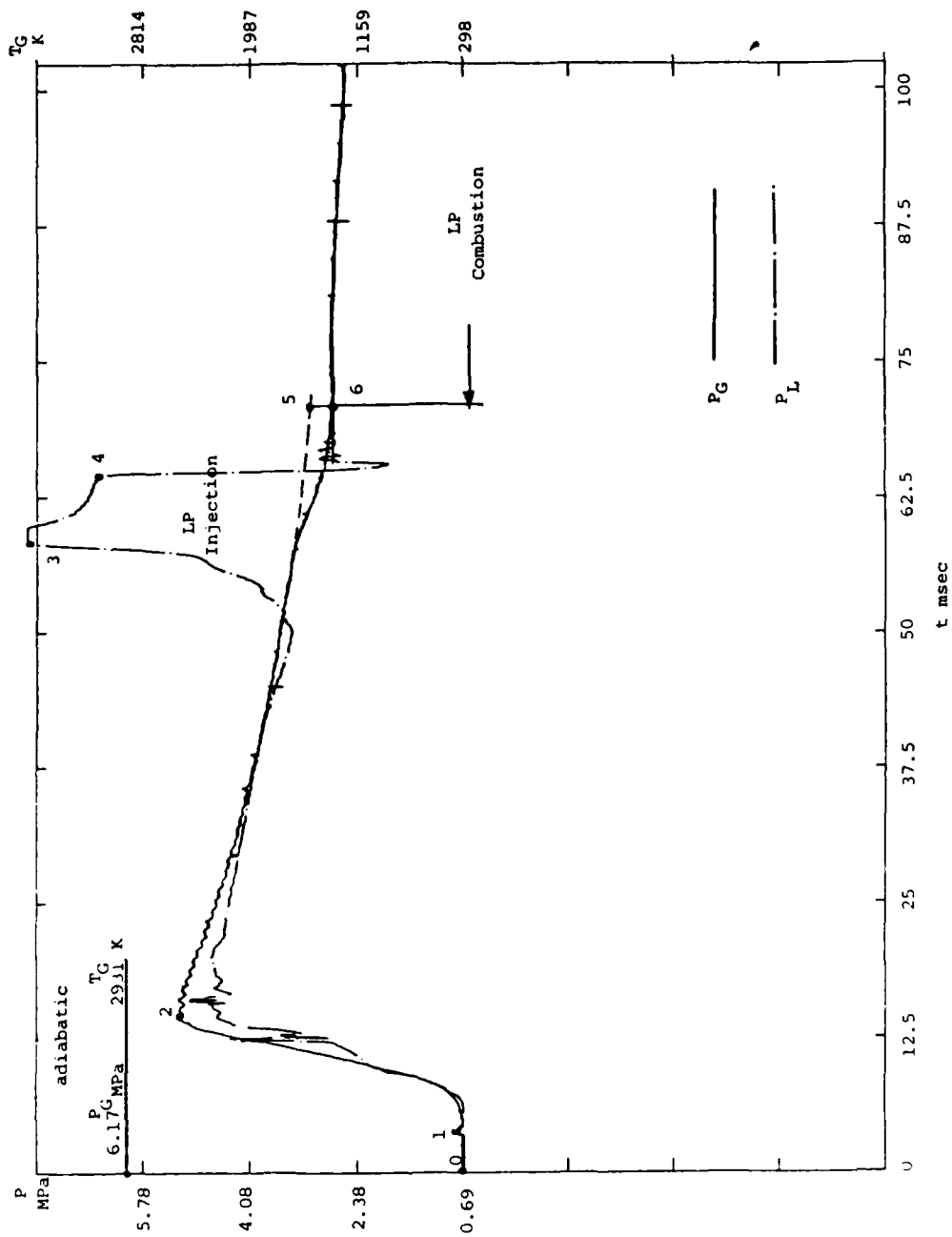


Figure 20a. Ignition Test 100C200I003S-a

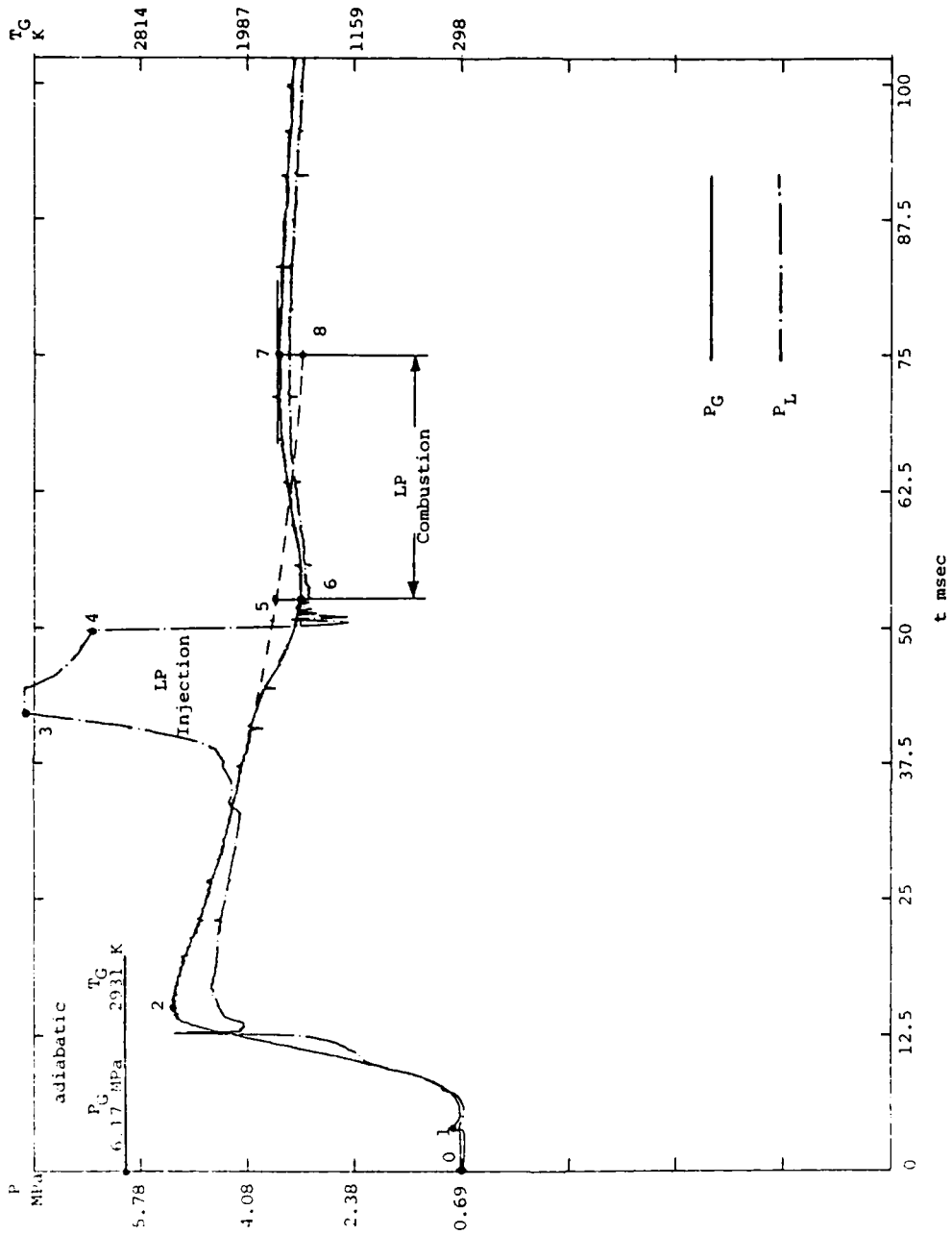


Figure 20b. Ignition Test 100C200I003S-b

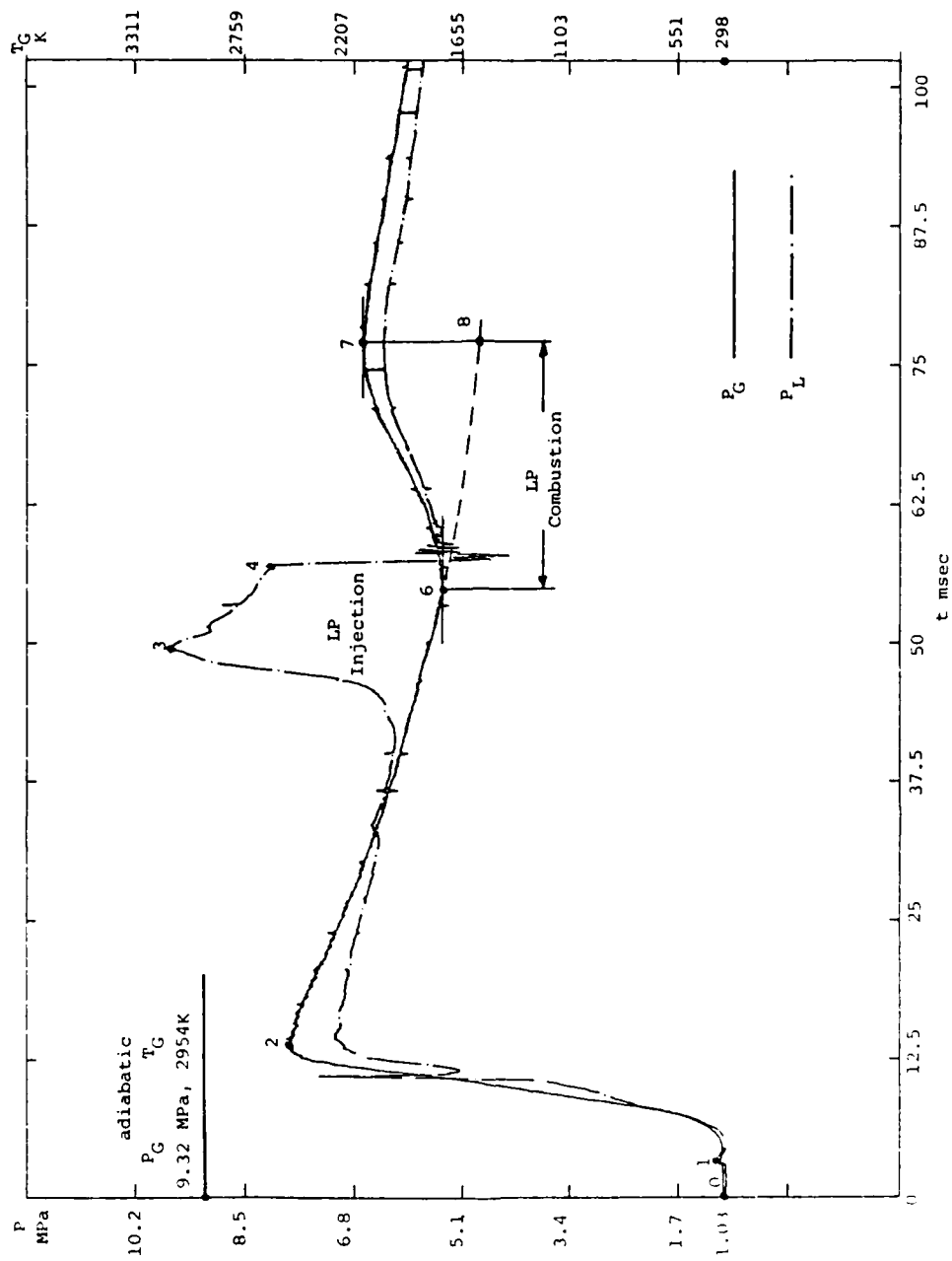


Figure 2la. Ignition test 150C250I003S-a

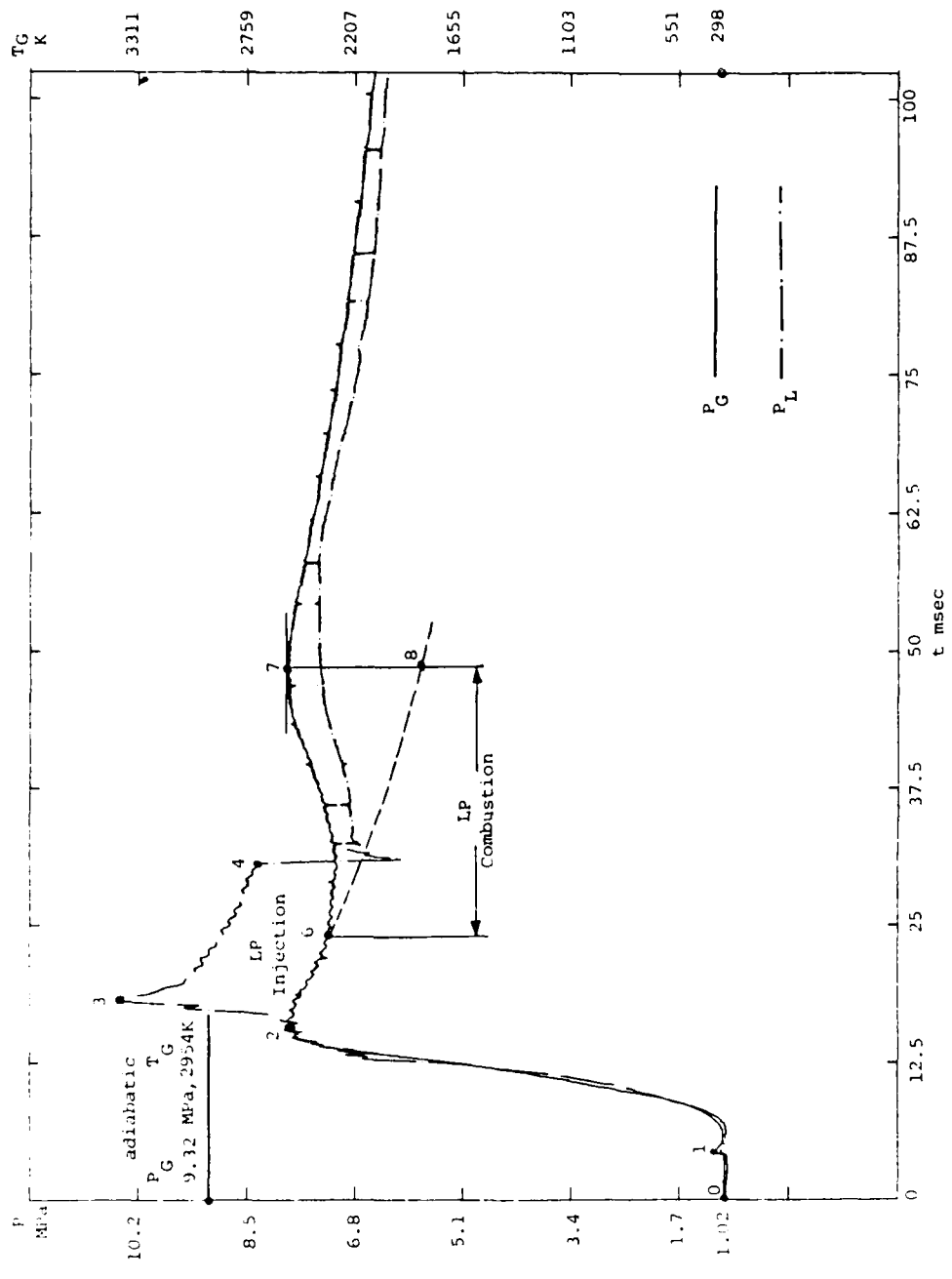
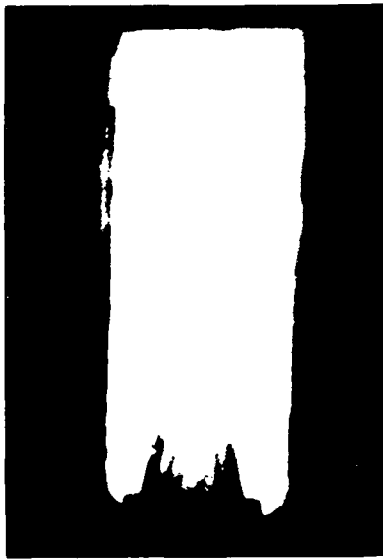
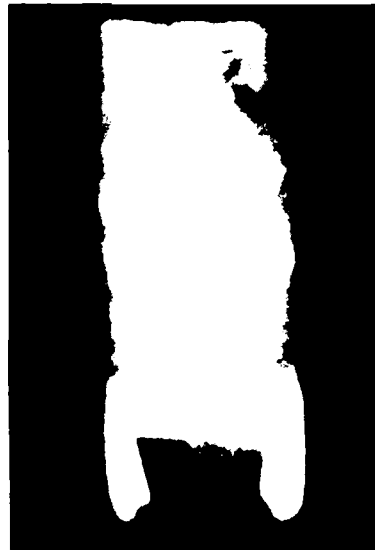
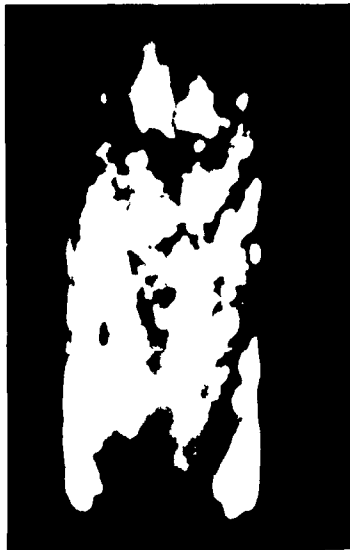


Figure 2lb. Ignition Test 150c250I003S-b



Left: .001S Nozzle
Right: .003S Nozzle

Figure 22. LP 1846 into 5.5 MPa, 1800K, 22% Water,
78% Argon, V=30 m/s



Left: .002S7 Nozzle
V=30 m/s
Right: .005M15 Nozzle
V=45 m/s

Figure 23. LP 1846 into Figure 22 Environment.



Left: Isooctane,
.005S Nozzle,
V=45 m/s
Right: LP 1846,
.020S Nozzle,
V=20 m/s

Figure 24. Figure 22 Environment

REFERENCES

1. Morrison, W.F., Knapton, J.D., and Klingenberg, G., "Liquid Propellants for Gun Applications," USA ARRADCOM Report ARBRL-TR-2632, Jan 1985.
2. Klingenberg, G., Knapton, J.D., and Travis, K. E., "A Study of Liquid Jets," U.S. Army Ballistic Research Laboratory Report ARBRL-MR-03203, Oct 1982.
3. Miesse, C.C., "Correlations of Experimental Data on the Disintegration of Liquid Jets," Indust. Engng. Chem., Vol. 47, p. 160, 1955.
4. Reitz, R.D., "Atomization and Other Breakup Regimes of a Liquid Jet," PhD Dissertation, MAE Report No. 1375-T, Princeton University, Princeton, NJ, Sep. 1978.
5. Wu, Ko-Jen, "Atomizing Round Jets," PhD Dissertation, MAE Report No. 1612-T, Princeton University, NJ, July 1983.
6. Bergwerk, W., "Flow Pattern in Diesel Nozzle Spray Holes," Proc. Instn. Mech. Engrs., Vol. 173, p.655, 1959.
7. Taylor, G.I., "Generation of Ripples by Wind Blowing over a Viscous Fluid," Collected Works of G. I. Taylor, Vol. 3., 1940.
8. Ranz, W.E., "Some Experiments on Orifice Sprays," Canad. J. Chem. Engrn., Vol 36, p. 175, 1958.
9. Abramowitz, G.N., "The Theory of Turbulent Jets," M.I.T. Press, 1963.
10. Beyer, R.A., "Atmospheric Pressure Studies of Liquid Propellant Drops in Hot Flows," to be published in the Proceedings of the 22nd JANNAF Combustion Meeting, 1985.
11. Williams, F.A., "Combustion Theory," Addison-Wesley Publication Co., 1965, Chapter 10.
12. Klein, N. and Sasse', R.A., "Ignition Studies of Aqueous Monopropellants," USA ARRADCOM Report ARBRL-TR-02232, April 1980.
13. Law, C.K., private communication of work conducted under contract DAAG29-81-D-0100, Aug 1985.
14. Hinze, J.O., "Turbulence," McGraw Hill, 1959.
15. Yuan, S.W., "Foundation of Fluid Mechanics," Prentice-Hall Inc, 1967, Chapter 8.
16. Giffen, E. and Muraszew, A., "The Atomization of Liquid Fuels," John Wiley and Sons, 1953.

17. Gordon, S. and McBride, B.J., "Computer Program for Calculations of Complex Chemical Equilibrium Compositions, Rocket Performance, Incident and Reflected Shocks and Chapman-Jouquet Detonations," NASA-SP-273, 1971 (1981 version).
18. Jost, Wilhelm, "Explosion and Combustion Processes in Gases," Chapter IV, McGraw Hill, 1946.
19. Faeth, G.M., "Evaporation and Combustion of Sprays," Prog. Energy Combust. Sci., Vol 9, 1983.

NOMENCLATURE

B	-	Ratio of Re to We
C_d	-	Drag coefficient
C_D	-	Discharge coefficient
C_p, C_v	-	Heat capacities
d_p	-	Particle size
D	-	twice the nozzle annulus gap
h	-	Heat transfer coefficient
K	-	Cavitation number
K_G	-	Heat conductivity of gas
L	-	Nozzle length
m	-	Mass
M	-	Molecular weight
P	-	Pressure
Pr	-	Prandtl number
R	-	Universal gas constant
Re	-	Reynolds number
t	-	Time
t_h	-	Inert heat-up time
t_m	-	Momentum transfer time
T	-	Temperature
V	-	Injection velocity
V_c	-	Combustor volume
We	-	Weber number
X_m	-	Most unstable wavelength
ρ	-	Density
μ	-	Viscosity

NOMENCLATURE (Con't)

- σ - Surface tension
- θ - Divergence angle of the jet

SUBSCRIPTS

- O - Initial conditions
- F - Flame
- G - Gas
- L - Liquid
- LG - Gas products of liquid
- V - Vapor

DISTRIBUTION LIST

<u>No. of Copies</u>	<u>Organization</u>	<u>No. of Copies</u>	<u>Organization</u>
12	Commander Defense Technical Info Center ATTN: DTIC-DDA Cameron Station Alexandria, VA 22304-6145	3	Director Benet Weapons Laboratory Armament R&D Center US Army AMCCOM ATTN: SMCAR-LCB-TL E. Conroy A. Graham Watervliet, NY 12189
1	Director Defense Advanced Research Projects Agency ATTN: H. Fair 1400 Wilson Boulevard Arlington, VA 22209	1	Commander US Army Armament, Munitions and Chemical Command ATTN: SMCAR-ESP-L Rock Island, IL 61299-7300
1	HQDA DAMA-ART-M Washington, DC 20310	1	Commander US Army Aviation Research and Development Command ATTN: AMSAV-E 4300 Goodfellow Blvd. St. Louis, MO 63120
1	Commander US Army Materiel Command ATTN: AMCDRA-ST 5001 Eisenhower Avenue Alexandria, VA 22333-0001	1	Director US Army Air Mobility Rsch. and Development Lab. Ames Research Center Moffett Field, CA 94035
13	Commander Armament R&D Center US Army AMCCOM ATTN: SMCAR-TSS SMCAR-TDC SMCAR-SCA, B. Brodman R. Yalamanchili SMCAR-LCA, D. Downs A. Beardell SMCAR-LCE, N. Slagg SMCAR-LCS, W. Quine A. Bracuti J. Lannon SMCAR-FSS-A, R. Price L. Frauen SMCAR-FSA-S, H. Liberman Dover, NJ 07801	1	Commander US Army Communications Electronics Command ATTN: AMSEL-ED Fort Monmouth, NJ 07703
		1	Commander ERADCOM Technical Library ATTN: STET-L Ft. Monmouth, NJ 07703-5301
		1	Commander US Army Harry Diamond Labs ATTN: DELHD-TA-L 2800 Powder Mill Rd Adelphi, MD 20783

DISTRIBUTION LIST

<u>No. of Copies</u>	<u>Organization</u>	<u>No. of Copies</u>	<u>Organization</u>
1	Commander US Army Missile Command Rsch, Dev, & Engr Ctr ATTN: AMSMI-RD Redstone Arsenal, AL 35898	1	Commandant US Army Armor Center ATTN: ATSB-CD-MLD Ft Knox, KY 40121
1	Commander US Army Missile & Space Intelligence Center ATTN: AIAMS-YDL Redstone Arsenal, AL 35898-5500	1	Commander US Army Development and Employment Agency ATTN: MODE-TED-SAB Fort Lewis, WA 98433
1	Commander US Army Belvoir R&D Ctr ATTN: STRBE-WC Tech Library (Vault) B-315 Fort Belvoir, VA 22060-5606	1	Commander Naval Surface Weapons Center ATTN: Code G33, J. East Dahlgren, VA 22448-5000
1	Commander US Army Tank Automotive Cmd ATTN: AMSTA-TSL Warren, MI 48397-5000	2	Commander US Naval Surface Weapons Ctr. ATTN: O. Dengel K. Thorsted Silver Spring, MD 20902-5000
1	Commander US Army Research Office ATTN: Tech Library P.O. Box 12211 Research Triangle Park, NC 27709-2211	1	Commander Naval Weapons Center China Lake, CA 93555-6001
1	Director US Army TRADOC Systems Analysis Activity ATTN: ATAA-SL White Sands Missile Range NM 88002	1	Commander Naval Ordnance Station ATTN: C. Dale Code 5251 Indian Head, MD 20640
1	Commandant US Army Infantry School ATTN: ATSH-CD-CSO-OR Fort Benning, GA 31905	1	Superintendent Naval Postgraduate School Dept of Mechanical Eng. ATTN: Code 1424, Library Monterey, CA 93943
1	Commandant US Army Field Artillery School ATTN: ATSF-CMW Ft Sill, OK 73503	1	AFWL/SUL Kirtland AFB, NW 87117
		1	Air Force Armament Lab ATTN: AFATL/DLODL Eglin, AFB, FL 32542-5000
		1	AFOSR/NA (L. Caveny) Bldg. 410 Bolling AFB, DC 20332

DISTRIBUTION LIST

<u>No. of Copies</u>	<u>Organization</u>	<u>No. of Copies</u>	<u>Organization</u>
1	Commandant USAFAS ATTN: ATSF-TSM-CN Ft Sill, OK 73503-5600	1	Calspan Corporation ATTN: Tech Library P.O. Box 400 Buffalo, NY 14225
1	US Bureau of Mines ATTN: R.A. Watson 4800 Forbes Street Pittsburgh, PA 15213	7	General Electric Ord. Sys Dpt ATTN: J. Mandzy, OP43-220 R.E. Mayer H. West M. Bulman R. Pate I. Magoon W. O'Connor 100 Plastics Avenue Pittsfield, MA 01201-3698
1	Director Jet Propulsion Lab ATTN: Tech Libr 4800 Oak Grove Drive Pasadena, CA 91109		
2	Director National Aeronautics and Space Administration ATTN: MS-603, Tech Lib MS-86, Dr. Povinelli 21000 Brookpark Road Lewis Research Center Cleveland, OH 44135	1	General Electric Company Armanent Systems Department ATTN: D. Maher Burlington, VT 05401
1	Director National Aeronautics and Space Administration Manned Spacecraft Center Houston, TX 77058	1	IITRI ATTN: Library 10 W. 35th St. Chicago, IL 60616
10	Central Intelligence Agency Office of Central Reference Dissemination Branch Room GE-47 HQS Washington, DC 20502	1	Olin Chemicals Research ATTN: David Gavin P.O. Box 586 Cheshire, CT 06410-0586
1	Central Intelligence Agency ATTN: Joseph E. Backofen HQ Room 5F22 Washington, DC 20505	2	Olin Corporation ATTN: Victor A. Corso Dr. Ronald L. Dotson P.O. Box 30-9644 New Haven, CT 06536
1	Central Intelligence Agency ATTN: Joseph E. Backofen HQ Room 5F22 Washington, DC 20505	1	Paul Gough Associates ATTN: Paul Gough PO Box 1614 Portsmouth, NH 03801
4	Bell Aerospace Textron ATTN: F. Boorady K. Berman A.J. Friona J. Rockenfeller Post Office Box One Buffalo, NY 14240	1	Safety Consulting Engr ATTN: Mr. C. James Dahn 5240 Pearl St. Rosemont, IL 60018

DISTRIBUTION LIST

<u>No. of Copies</u>	<u>Organization</u>	<u>No. of Copies</u>	<u>Organization</u>
1	Science Applications, Inc. ATTN: R. Edelman 23146 Cumorah Crest Woodland Hills, CA 91364	1	U. of Missouri at Columbia ATTN: Professor R. Thompson Department of Chemistry Columbia, MO 65211
1	Sunstrand Aviation Operations ATTN: Dr. Owen Briles P.O. Box 7002 Rockford, IL 61125	1	U. of Michigan ATTN: Prof. Gerard M. Faeth Department of Aerospace Engineering Ann Arbor, MI 48109-3796
1	Veritay Technology, Inc. ATTN: E. B. Fisher 4845 Millersport Highway, P.O. Box 305 East Amherst, NY 14051-0305	1	U. of Missouri at Columbia ATTN: Professor F. K. Ross Research Reactor Columbia, MO 65211
1	Director Applied Physics Laboratory The Johns Hopkins Univ. Johns Hopkins Road Laurel, Md 20707	1	U. of Missouri at Kansas City Department of Physics ATTN: Prof. R.D. Murphy 1110 East 48th Street Kansas City, MO 64110-2499
2	Director Chemical Propulsion Info Agency The Johns Hopkins Univ. ATTN: T. Christian Tech Lib Johns Hopkins Road Laurel, MD 20707	1	Pennsylvania State University Dept. of Mechanical Eng ATTN: K. Kuo University Park, PA 16802
2	University of Delaware Department of Chemistry ATTN: Mr. James Cronin Professor Thomas Brill Newark, DE 19711	2	Princeton Combustion Rsch Laboratories, Inc. ATTN: N.A. Messina M. Summerfield 475 US Highway One North Monmouth Junction, NJ 08852
1	U. of ILLinois at Chicago ATTN: Professor Sohail Murad Dept of Chemical Eng Box 4348 Chicago, IL 60680	1	University of Arkansas Department of Chemical Engineering ATTN: J. Havens 227 Engineering Building Fayetteville, AR 72701
1	U. of Maryland at College Park ATTN: Professor Franz Kasler Department of Chemistry College Park, MD 20742		

DISTRIBUTION LIST

<u>No. of Copies</u>	<u>Organization</u>	<u>No. of Copies</u>	<u>Organization</u>
--------------------------	---------------------	--------------------------	---------------------

Aberdeen Proving Ground

Dir, USAMSAA
ATTN: AMXSY-D
AMXSY-MP, H. Cohen

Cdr, USATECOM
ATTN: AMSTE-TO-F

CDR, CRDEC, AMCCOM
ATTN: SMCCR-RSP-A
SMCCR-MU
SMCCR-SPS-IL

USER EVALUATION SHEET/CHANGE OF ADDRESS

This Laboratory undertakes a continuing effort to improve the quality of the reports it publishes. Your comments/answers to the items/questions below will aid us in our efforts.

1. BRL Report Number _____ Date of Report _____

2. Date Report Received _____

3. Does this report satisfy a need? (Comment on purpose, related project, or other area of interest for which the report will be used.) _____

4. How specifically, is the report being used? (Information source, design data, procedure, source of ideas, etc.) _____

5. Has the information in this report led to any quantitative savings as far as man-hours or dollars saved, operating costs avoided or efficiencies achieved, etc? If so, please elaborate. _____

6. General Comments. What do you think should be changed to improve future reports? (Indicate changes to organization, technical content, format, etc.) _____

CURRENT
ADDRESS

Name

Organization

Address

City, State, Zip

7. If indicating a Change of Address or Address Correction, please provide the New or Correct Address in Block 6 above and the Old or Incorrect address below.

OLD
ADDRESS

Name

Organization

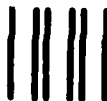
Address

City, State, Zip

(Remove this sheet along the perforation, fold as indicated, staple or tape closed, and mail.)

FOLD HERE

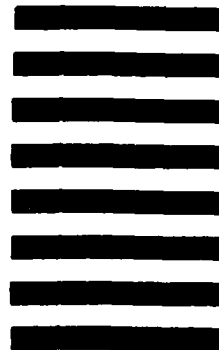
Director
U.S. Army Ballistic Research Laboratory
ATTN: SLCBR-DD-T
Aberdeen Proving Ground, MD 21005-5066



NO POSTAGE
NECESSARY
IF MAILED
IN THE
UNITED STATES

OFFICIAL BUSINESS
PENALTY FOR PRIVATE USE, \$300

BUSINESS REPLY MAIL
FIRST CLASS PERMIT NO 12062 WASHINGTON, DC
POSTAGE WILL BE PAID BY DEPARTMENT OF THE ARMY



Director
U.S. Army Ballistic Research Laboratory
ATTN: SLCBR-DD-T
Aberdeen Proving Ground, MD 21005-9989

FOLD HERE

END

5-87

DTIC